ALMA MATER STUDIORUM - UNIVERSITÀ DI BOLOGNA

SCHOOL OF ENGINEERING AND ARCHITECTURE

DEPARTMENT OF ELECTRICAL, ELECTRONIC AND INFROMATION ENGINEERING
"Guglielmo Marconi"
DEI

MASTER'S DEGREE IN
Telecommunications Engineering

MASTER'S THESIS
in
Software Development

Orthogonal chirp division multiplexing: performance evaluation in the presence of phase noise

PRESENTED BY:

Nicolò Longhi

SUPERVISOR:

Prof. Ing. Gianni Pasolini

CO-SUPERVISOR:

Dott. Ing. Giampaolo Cuozzo

Academic year
2020/2021

Call
II

Table of contents

Introduction

In Beyond 5G technologies, Terahertz communications will be used [1]: frequency bands between 100 GHz and 10 THz will be exploited in order to have higher throughput and lower latency. Those frequency bands suffer from several impairments, and it is thought that phase noise is one of the most significant. Orthogonal Chirp Division Multiplexing (OCDM) might be used in Beyond 5G communications, thanks to its robustness to multipath fading: it outperforms Orthogonal Frequency Division Multiplexing (OFDM) systems [2].

The aim of this thesis is to find a suitable model for describing phase noise in Terahertz communications, and to study the performance of an OCDM system affected by this impairment. After this, a simple compensation scheme is introduced, and the improvement that it provides is analysed.

The thesis is organized as follow: in the first chapter Terahertz communications and Beyond 5G are introduced, in the second chapter phase noise is studied, in the third chapter OCDM is analysed, and in the fourth chapter numerical results are presented.

1. Introduction to Beyond 5G and THz communications

In the last 30 years, cellular communications have revolutionized our world. Second generation mobile networks (2G), first introduced in 1991, were the first digital cellular networks, allowing a higher security and capacity with respect to analog ones. It was possible to make phone calls and send messages. The introduction of third generation networks (3G) enabled faster data transfer, allowing the access to the Internet and to share files. When those networks were fully established, the first smartphones were released, and together with fourth generation networks (4G), which allowed a much higher throughput and lower latency, they set the basis for the App Economy and the advent of social media. According to the latest Ericsson Mobility Report (June 2021) [3], there are around 8 billion mobile subscriptions worldwide and at the end of 2020 there were 6 billion smartphone subscriptions. As reported by GSMA in "The Mobile Economy 2021" report [4], "In 2020, mobile technologies and services generated 5.1% of global GDP".

We are witnessing to the dawn of 5G era, and it is thought it will have a disruptive effect on our life and society. This technology, whose adoption and development have been delayed due to the pandemic, will allow a higher throughput (peak data rate up to 20 Gbit/s) and much lower latency (down to 1 ms) [5]: this will enable mobile cloud computing and augmented and virtual reality. 5G will be not only a network for human communications, but it is designed to make things communicate: this will allow an huge leap for IoT. Vehicular communications, industrial IoT (IIoT), smart cities, smart agriculture will be benefited by this technology.

The ongoing Fourth Industrial Revolution, which is based on the interconnection between machines, the exchange and exploitation of information for manufacturing, will be strongly pushed by 5G. 5G addresses three different use cases: enhanced mobile broadband (eMBB), massive machine type communications (mMTC) and ultra-reliable low latency communications (URLLC). As shown in [6], the set of industrial use cases is heterogenous, there are very different requirements for the "Factory of The Future". As reported in [7], [8], some of those services require a reliability up to 99.999999% and a cycle time lower than 0.5 ms (and an even lower transmission time). Those requirements cannot be fulfilled by 5G: as

shown in [9], 3GPP Release 16 provides a reliability up to 99.9999% and a latency down to 1 ms. Only Beyond 5G communications will fulfil those requirements, most likely 6G.

This is one of the reasons why there will be Beyond 5G technologies, because the need to satisfy stricter QoS requirements. Another reason is that traffic demand has a fast-paced growth: as shown in [10], at the end of 2020 total global mobile data traffic reached 49 EB (1 EB = 10^{18} bytes) per month, and it is foreseen it will reach 237 EB per month in 2026. This means that also the average network throughput will increase. As shown in the report "The 5G opportunity – how 5G will solve the congestion problems of today's 4G networks" [11], 4G networks are congested and they struggle to provide consistent performance. 5G is thought it will solve this issue, but due to the foreseen traffic growth it might struggle in the future.

While current generation technologies' performances have been boosted by the exploitation of millimetre wave (mmWave) frequency bands (between 30 GHz and 300 GHz), in particular the ones below 100 GHz, it is thought that the technology that will be used in Beyond 5G networks in order to satisfy the aforementioned requirements is Terahertz communications [1], which exploits radio frequency bands between 100 GHz and 10 THz [12]. This band, between radio and optical bands, is still unused and it theoretically allows the use of huge bandwidths, up to several THz, that would make possible capacity in the order of Terabits per second. Terahertz bands are the less studied part of the electromagnetic spectrum, so they need to be deeply investigated in order to understand how to exploit them. Due to the physical characteristics of such bands, it is possible to use both electronics and photonics technologies: it is thought that new devices will be used, like gallium arsenide and indium phosphide electronics, as well as silicon-based technologies, and more exotic materials could be exploited, like graphene [12].
Besides huge bandwidths, Terahertz bands allow to have non-line-of-sight (NLoS) propagation, a strong advantage over optical communications, while having a high directionality, that increase security by lowering eavesdropping chances [12].

It is fundamental to find a suitable model to describe the behaviour of the channel. At those frequencies, due to the presence of water vapor molecules, it is present a strong atmospheric absorption, as shown in Figure 1: this is the reason why this channel is considered highly frequency selective. Moreover, it is present a tremendous path loss attenuation, as it is

possible to see in Figure 2, due to the quadratic dependency on the operating frequency, but this effect could be mitigated by using beamforming techniques.

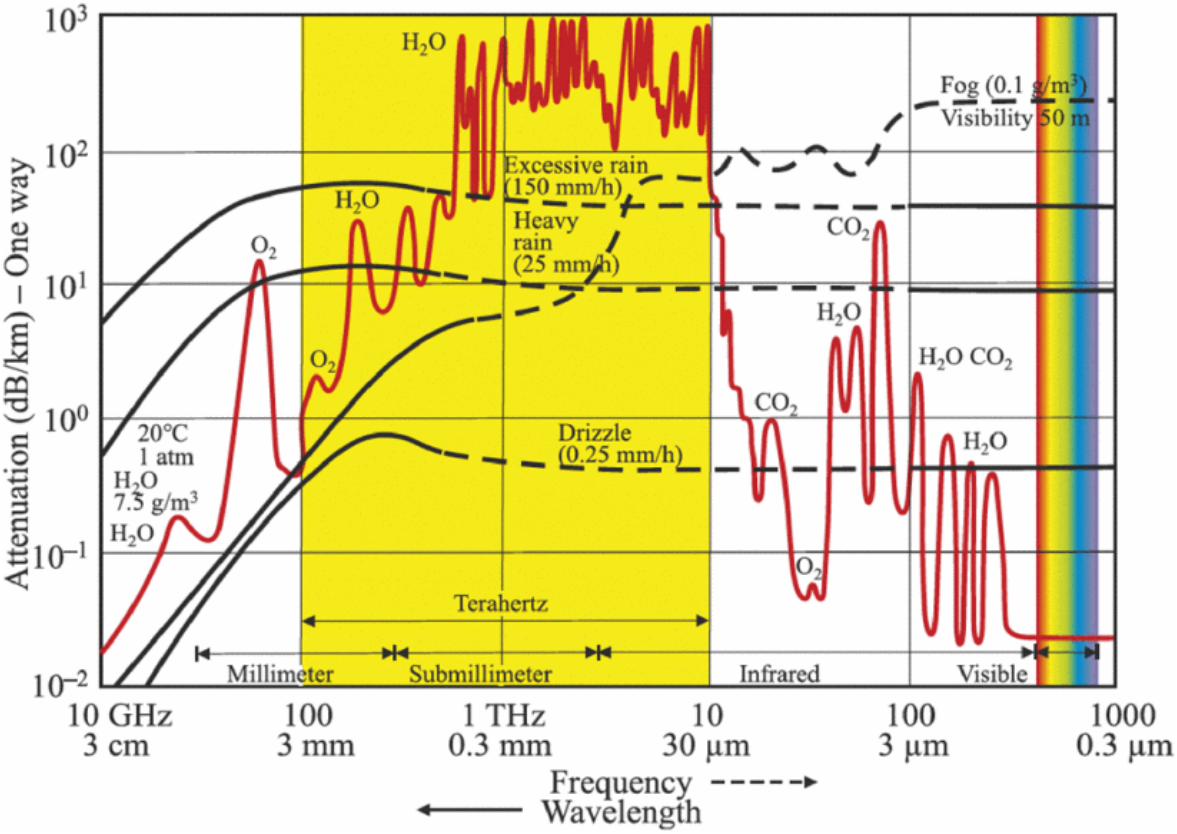

Figure 1: Comparison between the attenuation impact of different environmental effects on different frequency bands [12]

As highlighted in [13], molecular absorption also introduce noise, since when an electromagnetic wave collides with a molecule it makes it vibrate, and this vibration turns into an electromagnetic radiation with the same frequency as the incident one. This phenomenon should be carefully taken into account, because it deteriorates performance, and it determines the channel capacity.

As reported in the 2021 Fourth IEEE International Workshop on Mobile Terahertz Systems (IWMTS), it is thought that phase noise will be one of the main impairments, due to the high operating frequency and the wide bandwidth. This phenomenon is the one that will extensively be discussed and studied in this thesis.

While the aforementioned problems were related to the physical layer, there are also problems related to medium access control (MAC) protocols [14] due to the antenna directionality and the fact that propagation delays at those frequencies are comparable to the transmission time

of packets [15]. Classical MAC protocols cannot cope with those phenomena, and ad hoc solutions must be found.

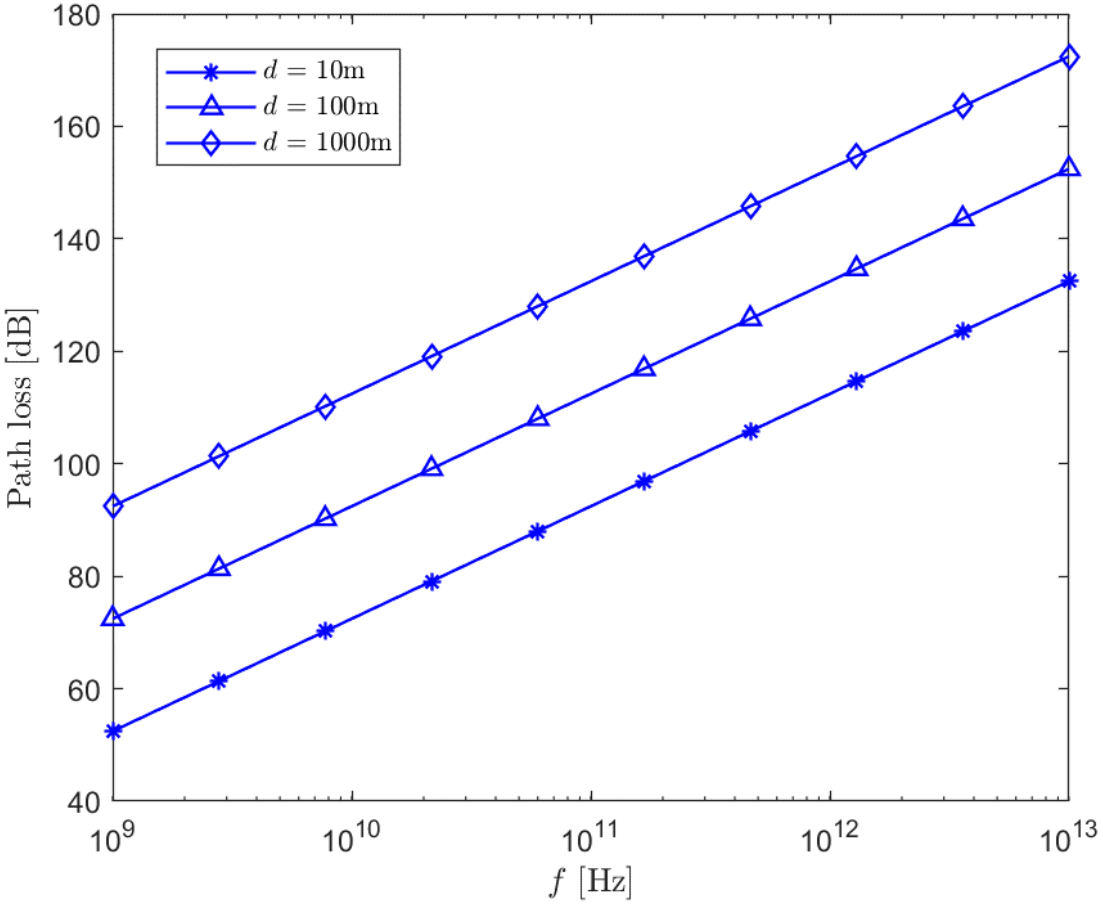

Figure 2: Free space path loss between 1 GHz and 10 THz, at distances of 10m, 100m and 1000m.

THz communications need to be deeply studied, in order to be able to provide the performance needed in the future. But what are those performance for? Previously it has been mentioned that Beyond 5G technologies will be able to provide a higher network throughput and they will satisfy stricter QoS requirements: IIoT will be strongly improved by latency down to hundreds of microseconds and improved vehicular communications will allow a higher safety and better autonomous driving, but those applications are available now, obviously with lower performances. There are some new applications that will be potentially made possible thanks to Beyond 5G technologies and Terahertz communications [16], [17], [18]:

- Accurate Indoor Positioning: Global Navigation Satellite Systems (GNSSs) are mature and allow a high accuracy, while on the opposite Indoor Positioning Systems (IPSs)

need to be strongly improved. The huge bandwidth that will be provided by THz communications could revolutionize IPS.

- Holographic communications: instead of video calls, in the future we might communicate with holograms, providing a richer experience. This would need an extremely high throughput.
- Tactile communications: while vision will be enriched by holograms, also other senses could be involved in remote communications, like touch. We will be able to physical interact thought the Internet, but this requires new networks, since higher throughput and lower latency are mandatory.
- Datacentre connectivity: nowadays, interconnections in datacentres are realized through wires. Due to the increasing demand for storage and data processing, they are more and more used, and networks are becoming more complex. Wired networks are expensive, not flexible, and static. Wireless technology could solve those issues, but only Beyond 5G technologies will provide a throughput high enough.
- Wireless Intra-Chip communications: in order to improve computational capabilities, CPUs are evolving by increasing core numbers rather than increasing operating frequency. The interconnections have become more and more complex, facing topology and routing issues. Wireless communications can help solving those problems, but extremely small transceivers are needed, that can be realized only if THz bands (or even higher frequency) are used: multicore wireless Network-on-Chip will most probably be possible thanks to Terahertz communications.

Those are just some of the applications that it is thought will be made possible by Beyond 5G and Terahertz communications: several others will certainly come when those technologies will be available.

2. Discussion on phase noise in THz communications

Every electronic component is non-ideal: the actual behaviour is different from the one predicted and every model that describe how they work is just an approximation. Oscillators are one of the fundamental circuits of every communication system, and phase noise is a physical problem that arise from their non-ideal behaviour.

The ideal output, in the time domain, of an oscillator is:

$$v(t) = A \cdot cos(2\pi f_0 t + \phi_0), \tag{2.1}$$

where A is amplitude and ϕ_0 is a constant phase offset. Instead, the real behaviour is:

$$v(t) = A(t) \cdot cos\big(2\pi f_0 t + \phi(t)\big), \tag{2.2}$$

where $A(t)$ is the amplitude noise and $\phi(t)$ is the phase noise. As shown in [19], while the amplitude noise can be practically eliminated by using amplitude limiting mechanism, the phase noise cannot be completely removed. Due to this phenomenon, the power spectrum density (PSD) is not just a Dirac delta on the fundamental frequency, but there are also unwanted components, as shown in Figure 3.

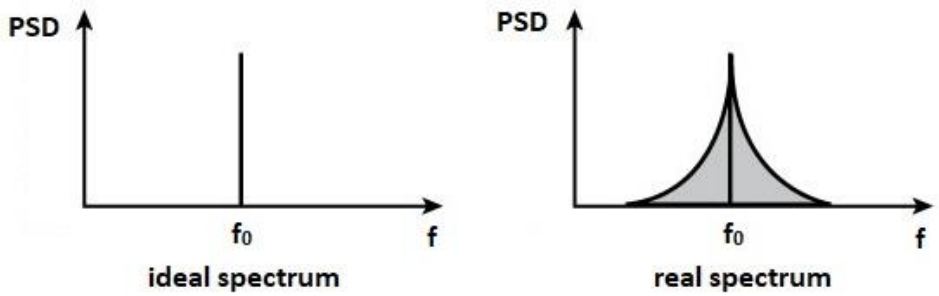

Figure 3: Comparison between the ideal spectrum and the real spectrum of an oscillator

2.1 Phased locked loop

Phased locked loops (PLL) are electronic circuits widely adopted in telecommunications. They are used in oscillators because they allow to have a high operating frequency while keeping the quality factor Q high enough. Their scheme is the following:

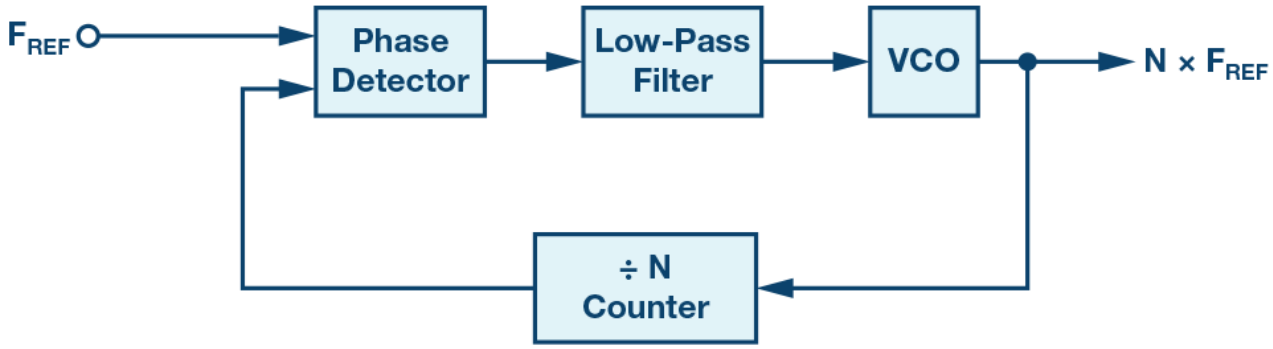

Figure 4: PLL fundamental scheme. Image from https://www.analog.com/en/analog-dialogue/articles/phase-locked-loop-pll-fundamentals.html

The first element is a phase detector, which has in input a reference signal and the feedback signal, and provides in output a signal that, after being filtered, is proportional to their phase difference. This signal drives the Voltage Controlled Oscillator (VCO), that produces a frequency that depends on its input. Let us ignore the divider and let us assume the feedback signal is equal to the output signal: if at the phase detector the phase difference is zero, the system is steady, instead if it is different from zero the system is unstable, and the signal generated by the phase detector drives the VCO in such a way to make the output frequency converge to the input frequency. If we introduce the divider, the output tends to converge to a signal whose frequency is *N* times the input one. Usually, the reference signal is generated by an accurate quartz crystal oscillator, which has a high *Q*, in order to have at output a signal with a *Q* relatively high.

In order to have a frequency suitable for THz communications, usually several PLL stages are used in cascade, if the oscillator is realized with RF components instead of optical ones. As reported in [20], the digital multiplication of the frequency by *M* rises the signal's phase noise level by $20 * log_{10}(M)\ dB$, and it should be carefully taken into account.

In order to characterize the phase noise, it is important to highlight that the VCO behaves as an integrator in the phase domain.

2.2 Phase noise characterization

As reported in IEEE Standard Definitions [21], in order to characterize phase noise, the most used figure of merit is $\mathcal{L}(f)$, defined as one half of the one-sided spectral density of the phase fluctuations:

$$\mathcal{L}(f) = \frac{1}{2}\,\mathcal{S}_\phi(f). \tag{2.3}$$

The old definition was:

$$\mathcal{L}(f) = \frac{power\ density\ in\ one\ phase\ noise\ modulation\ sideband, per\ Hz}{total\ signal\ power} = \\ = \frac{\mathcal{S}_v(f + f_0)}{P_v}, \tag{2.4}$$

where $\mathcal{S}_v$ is the power spectral density and P_v is the power of the oscillator output. When expressed in decibels, its units are dB below the carrier in a 1 Hz bandwidth (dBc/Hz), as shown in Figure 5. Considering the old definition, the relation between $\mathcal{L}(f)$ and $\mathcal{S}_\phi$ is:

$$\mathcal{L}(f) \cong \frac{1}{2}\,\mathcal{S}_\phi(f). \tag{2.5}$$

This expression is valid when the power of the phase noise is "small enough" and f_0 "high enough" [22].

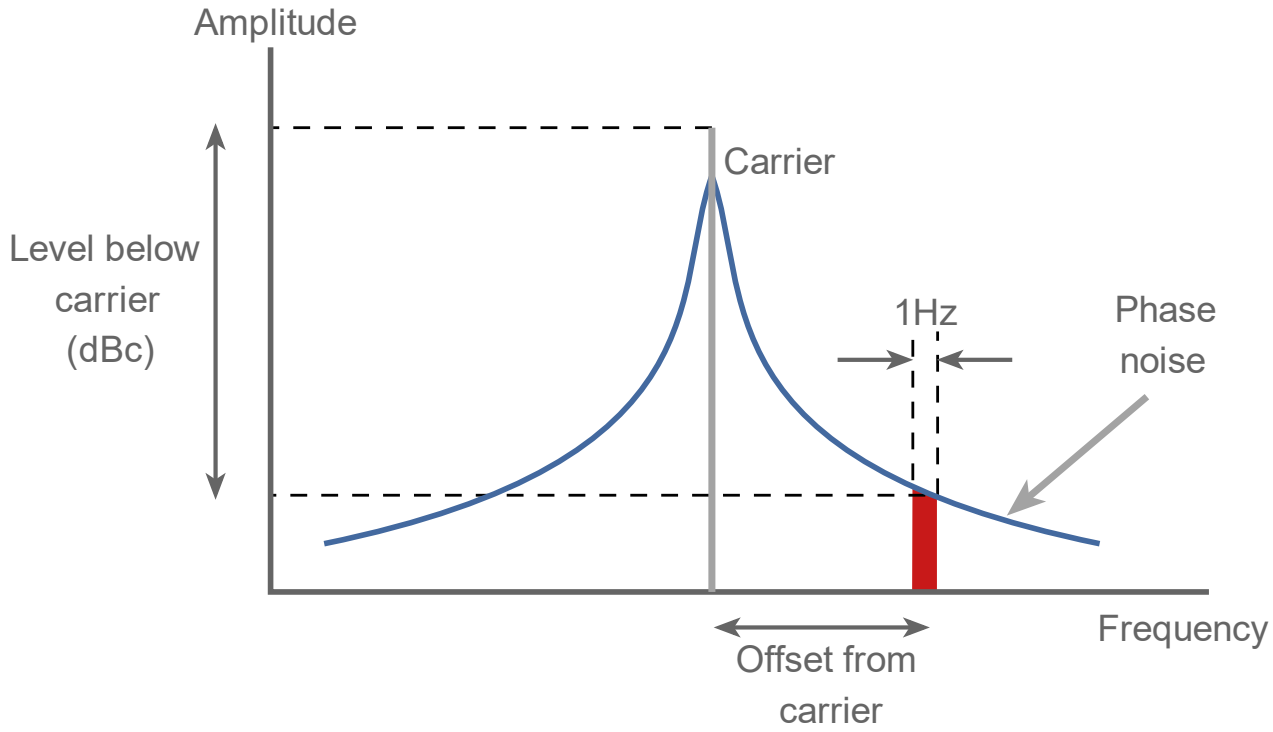

Figure 5: Graphical representation of dBc/Hz definition. Image from https://www.electronics-notes.com/images/noise-phase-specification-01.svg

(2.4) allows to have a simpler definition, and this is the reason why it is used in every paper which deals with phase noise. The problem is to find a correct expression for $\mathcal{S}_\phi$, since (2.5) could lead to incorrect results. In [23] it is shown how it is computed, but firstly it is necessary to understand which are the inputs and the outputs of an oscillator and their characterization.

2.3 Phase noise origin

Oscillators' phase noise is generated inside their circuits, due to an integration mechanism of white (uncorrelated) and coloured (correlated) noise sources, as shown in [19], [23]. As reported in [24], the output of a voltage-controlled oscillator is:

$$y(t) = A \cdot \cos(\, 2\pi f_{fr} t \; + \; K_{VCO} \cdot \int_{-\infty}^{t} x(\tau) \; d\tau \,) \tag{2.6}$$

where f_{fr} is the free-running frequency, K_{VCO} is the "gain" of the VCO, and $x(\tau)$ is the input control voltage in the time domain. In a phase-locked loop, at the input of the VCO there is the phase difference between the reference source and the output (we are ignoring, for the sake of simplicity, the divider), that could be realized using a mixer. This is not the only component of $x(\tau)$: there are also noise sources that are integrated by the VCO, and this generates the phase noise. It is obvious that phase noise has a cumulative nature, due to the integration. As reported in [25], it is possible to write the phase noise as:

$$\phi(t) = \int_{0}^{t} \Phi(\tau) \; d\tau, \tag{2.7}$$

where $\Phi(\tau)$ is the superposition of every noise source, and then we can write the increment of phase noise over a time delay *T* as:

$$\Delta(t, \tau) = \phi(t) \; - \; \phi(t - T) = \int_{t-T}^{t} \Phi(\tau) \; d\tau. \tag{2.8}$$

This is usually called the phase noise increment process.

The integration process of white noise generates a component of $\mathcal{L}(f)$ with a slope of -20 dB/decade, while if we integrate a coloured noise whose PSD has a $1/f$ dependency, we obtain a component of $\mathcal{L}(f)$ with a slope of -30 dB/decade. There is a noise floor in $\mathcal{L}(f)$,

that is generated by amplifying / attenuating the white noise sources at the input. The following scheme sum up phase noise generation mechanisms [25].

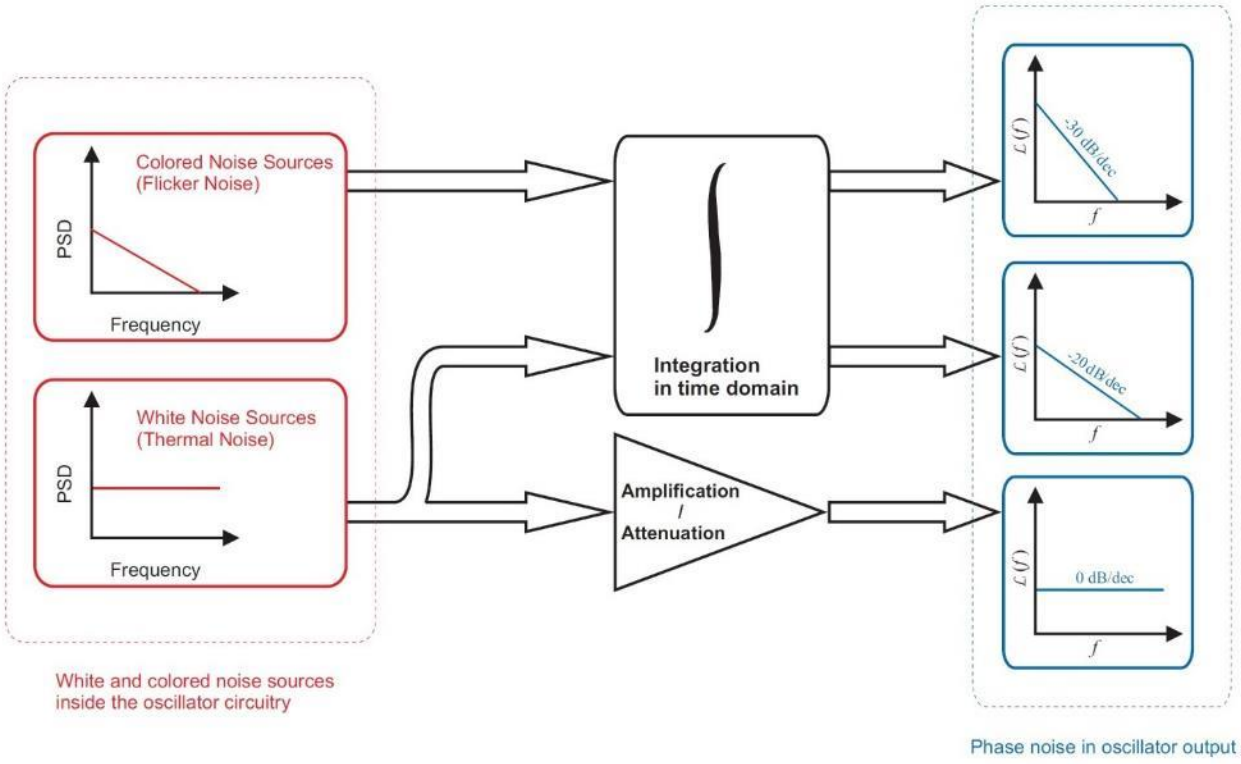

Figure 6: Phase Noise generation mechanism [25]

2.4 Phase noise model

First of all, it is necessary to understand which are the noise sources that are in the oscillator. Thermal noise, that is caused by the thermal agitation of electrons inside conductors, at RF frequency is modelled as an ergodic Gaussian white process [26]. This should be carefully analysed at THz frequency: the accurate expression of the power spectrum of thermal noise is

$$\mathcal{G}_e(f) = \frac{2 \cdot R \cdot \hbar \cdot |f|}{e^{\frac{\hbar \cdot |f|}{k \cdot T}} - 1}, \tag{2.9}$$

where R is the resistor on which the noise is generated, T is the temperature of the resistor, $\hbar$ is Planck's constant and k is the Boltzmann constant. At RF frequency is valid the following approximation, using Taylor series:

$$e^{\frac{\hbar \cdot |f|}{k \cdot T}} - 1 \approx \frac{\hbar \cdot |f|}{k \cdot T}, \qquad when \ \frac{\hbar \cdot |f|}{k \cdot T} \ll 1, \tag{2.10}$$

so, we can approximate (2.9) as:

$$\mathcal{G}_e(f) \approx \frac{2 \cdot R \cdot \hbar \cdot |f|}{\frac{\hbar \cdot |f|}{k \cdot T}} = 2 \cdot R \cdot k \cdot T, \tag{2.11}$$

so, the power spectrum could be approximated as white. If we assume $T = 290\ K$, we get:

$$|f| \ll \frac{k \cdot T}{\hbar} \approx 6\ THz, \tag{2.12}$$

this means that (2.11) is valid when the operating frequency is much smaller than 6 THz. This is clearly true at RF (below 300 GHz), but this is not always true at THz frequency, so the thermal noise is coloured.

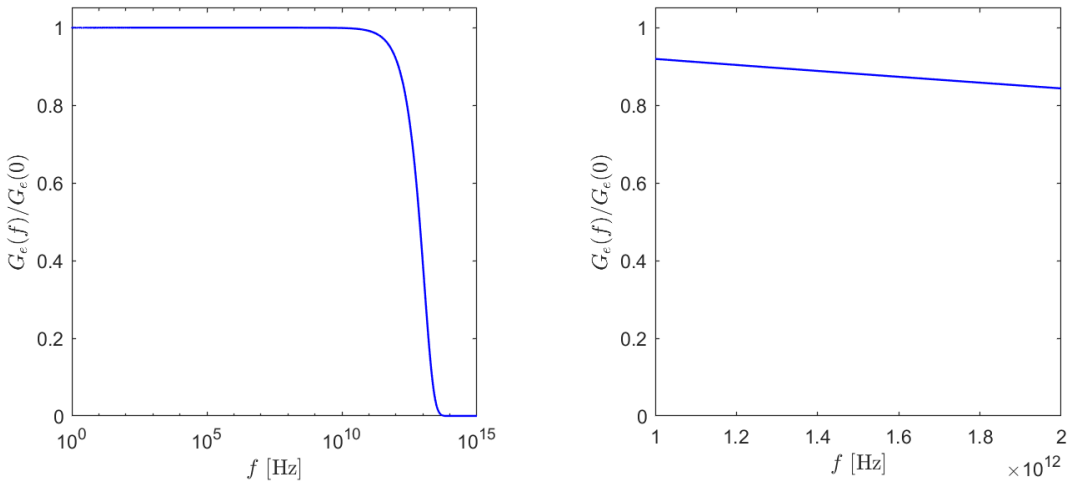

Figure 7: Normalized power spectrum of thermal noise, T = 290 K

In Figure 7, on the left it is present the graph of the normalized power spectrum of thermal noise, from 1 Hz to 1 PHz (the x axis has a logarithmic scale), and it is possible to appreciate the coloured nature of the spectrum. If we analyse the normalized spectrum around 1.5 THz in a frequency range of 1 THz (Figure 7 on the right), it can be seen that it changes slowly: if the bandwidth is relatively small (smaller than 100 GHz), we can assume that the power spectrum is constant in that band, so we can assume that the thermal noise is white.

Another source of noise is the one generated by molecular absorption, usually called molecular absorption noise. This phenomenon needs further research since it is a novelty in

wireless communications, but preliminary results show that it could be modelled as a Gaussian white process.

Those two are the main noise sources in a Terahertz communication system. There could be additional noise sources, like flicker noise, but usually they can be ignored. Let us assume that flicker noise is present: its spectrum is coloured, and it is proportional to $1/f$ (indeed, it is called also $1/f$ noise). Due to this characteristic, it is significant at low frequencies, and it affects only a tiny amount of bandwidth: for example, the corner frequency (the frequency value where white noise and flicker noise have the same PSD) in a FET transistor is in the order of some MHz. Since one of the benefits of using THz communications is the possibility to use several GHz wide bandwidths, it is possible to neglect this kind of noise.

It has been concluded that the noise sources in the oscillator could be modelled as white and Gaussian. Now, we are able to discuss on which model is the more appropriate for describing phase noise. There is a wide range of available models: some are simple, like uncorrelated Gaussian phase noise model, which is not very demanding from the computational viewpoint, but it could lead to inaccurate results, and some are quite complex, like the one proposed in [25], that leads to more reliable results, but on the other hand it is computational demanding. The main reason that drives to more complex models is the necessity to consider coloured noise sources: as described before, the VCO performs an integration in the phase domain, which causes the presence of a correlated output. If the input noise is already correlated, the output will be even more correlated, leading to the necessity of a complex model. As said before, we can assume the noise sources as white, and we can use a relatively simple model.

Assuming the system ideally equalized and synchronized in both time and frequency [22], they m-th received symbol can be written as

$$r_m = s_m e^{j\phi_m} + w_m, \tag{2.13}$$

where s_m is the m-th modulated symbol, ϕ_m is the phase noise that affects it, and $w_m \sim \mathbb{C}\mathcal{N}(0, \sigma_N^2)$ is the complex Gaussian noise, with zero mean and standard deviation σ_N.

The chosen model used to describe phase noise is the model that consider the superposition of a Wiener process and uncorrelated Gaussian process [22]

$$\phi_m = \phi_{w,m} + \phi_{g,m}. \tag{2.14}$$

A Wiener process is the process that is obtained by integrating white noise [23], so it is used to model the integration performed by the VCO. The phase noise samples of the Wiener phase noise are defined by:

$$\phi_{w,m} = \phi_{w,m-1} + \delta\phi_{w,m}, \tag{2.15}$$

where

$$\delta\phi_{w,m} \sim \mathcal{N}(0, \sigma_w^2). \tag{2.16}$$

This nomenclature indicates that $\delta\phi_{w,m}$ has a Gaussian distribution, with zero mean and standard deviation σ_w.

We can see that (2.15) is the discrete time version of (2.8) with a specific distribution, in particular:

$$\Delta(t,\tau) \leftrightarrow \delta\phi_{w,m}. \tag{2.17}$$

The uncorrelated Gaussian phase noise instead is defined as:

$$\phi_{g,m} \sim \mathcal{N}\left(0, \sigma_g^2\right), \tag{2.18}$$

and describes the phase noise generated by the amplification/attenuation of the white noise at the input.

As reported in [23], the output of an integrator with a white noise input is not stationary (indeed, it is modelled as a Wiener process). Due to this, we cannot model this system as Linear and Time Invariant (LTI): it is possible to understand it considering a reductio ad absurdum. As shown in [23], if we assume the system LTI, this leads to a spectrum $\mathcal{S}_\phi$ proportional to $1/f^2$, and if we compute the power as the integral of the power spectral density, we will obtain infinite power. The correct characterization of the process starts from the consideration that the increments of the Wiener process are stationary. This allows us to compute the power spectral density of the increments assuming an LTI system, and we find that the variance of the Wiener increments is

$$\sigma_w^2 = 4\pi^2 K_2 T, \tag{2.19}$$

where T is the symbol time.

This variance is related to the uncorrelated Gaussian one through the corner frequency, in particular

$$f_c^2 = K_2 / K_0, \tag{2.20}$$

where K_0 is the constant value of the power spectral density of the white Gaussian phase noise.

3. OCDM

In order to cope with frequency selective channels, multi-carrier transmissions have been introduced. The bit stream is divided in *P* parallel streams, each one with a smaller bit rate, and each one is modulated with a different carrier, then they are sent in parallel. When *P* is big enough, frequency selectivity could be neglected: the bandwidth of each stream is much smaller than the coherence bandwidth of the channel, so each stream is affected by flat fading. This solution has two problems:

1) Guard bands between carriers are needed, there is a loss of spectral efficiency;
2) If *P* is large, several modulators with very precise operating frequency are needed.

Those have been solved by implementing Orthogonal Frequency Division Multiplexing (OFDM) through Inverse Discrete Fourier Transform (IDFT). Using OFDM, guard intervals are not needed, and modulators have been substituted by IDFT: actually, Inverse Fast Fourier Transform (IFFT) algorithm is used.

OFDM maximize the spectrum efficiency of Frequency Division Multiplexing (FDM). Similarly, Orthogonal Chirp Division Multiplexing (OCDM) maximize the spectrum efficiency of Chirp Spread Spectrum (CSS).

Chirps are waveforms with several applications [2]: for example, they are used in radar systems and in communications systems. They are sinusoids whose frequency changes with time, based on the application: for example, in digital communication systems information could be encoded in the frequency sweep. CSS is a spread-spectrum modulation, therefore it has a wideband spectrum that provides excellent performances against frequency selective fading, and it allows to communicate in channels affected by strong noise. The drawback is that, due to the large occupied bandwidth, it has a low spectrum efficiency.

OCDM allows [2] to multiplex orthogonally chirped waveforms: they are sent on the same time interval and on the same bandwidth, without interfering, and they are generated digitally; both the amplitude and the phase of each chirp can be modulated.

OCDM could be potentially used in Beyond 5G communications since it outperforms OFDM under frequency selective channels [27], furthermore it can be generated starting from a DFT, so digital signal processing realized for OFDM can be exploited [28].

The following three sub-paragraphs come from internal documentation, on research carried by Professor Gianni Pasolini and Giampaolo Cuozzo, PhD Student at University of Bologna. In the fourth I will derive analytically the two components of the received OCDM signal affected by phase noise, and in the fifth a simple compensation scheme is described.

3.1 OCDM: Signal analysis

To understand the principles of the orthogonal chirp division multiplexing (OCDM) modulation, it is useful to relate it to the better known OFDM modulation, as they are both based on the parallel transmission of orthogonal signals with overlapping spectra. For both modulations, the complex envelope of the overall signal can be written as

$$i(t) = \sum_{n} \sum_{k=0}^{N-1} x_k(n) \psi_k(t - nT) g_T(t - nT) \tag{3.1}$$

where

- the index *n* refers to the *n*th chirp-interval,
- $\psi_k(t)$ represents the *k*th waveform of a set $\Psi = \{\psi_k(t)\}_{k=0}^{N-1}$ of mutually orthogonal waveforms,
- $N = |\Psi|$ is the number of orthogonal waveforms in Ψ,
- $x_k(n)$ is the complex symbol transmitted in the *n*th chirp-interval by the *k*th waveform,
- T is the symbol duration,
- $g_T(t)$ is the indicator function: $g_T(t) = 1$ for $0 \leq t < T$ and $g_T(t) = 0$ elsewhere.

In the case of OFDM signals, Ψ is a set of (complex) orthogonal carriers, usually dubbed subcarriers, defined as

$$\Psi = \{\psi_k(t)\}_{k=0}^{N-1} = \{e^{j2\pi k \Delta f}\}_{k=0}^{N-1} \tag{3.2}$$

with $\Delta f = \frac{1}{T}$, whereas for OCDM signals Ψ is a set of (complex) chirps,

$$\Psi = \{\psi_k(t)\}_{k=0}^{N-1} = \{e^{j\frac{\pi}{4}} e^{-j\pi \frac{B}{T}(t - \frac{k}{B})^2}\}_{k=0}^{N-1} \tag{3.3}$$

with *B* defined as $B \triangleq \frac{N}{T}$.

It can be readily proved [2] that the chirp waveforms $\psi_k(t)$ in (3.3) are mutually orthogonal,

as are the subcarriers in (3.2). The shape of the generic chirp $\psi_k(t)$ can be investigated by deriving its frequency deviation over time. In particular, given

$$\psi_k(t) = e^{j\frac{\pi}{4}} e^{-j\pi\frac{B}{T}\left(t-\frac{k}{B}\right)^2} = e^{j\vartheta_k(t)} \quad k \in [0, 1, \dots N-1] \tag{3.4}$$

it follows that the instantaneous frequency deviation of the *k*th chirp is

$$\Delta f_k(t) = \frac{1}{2\pi}\frac{d\vartheta_k(t)}{dt} = \frac{k}{T} - \frac{B}{T}t \tag{3.5}$$

As it turns out, the instantaneous frequency deviation of the OCDM chirp waveform $\psi_k(t)$ covers an interval *B* in the chirp-interval [0 *T*], being *T* the chirp duration, decreasing linearly starting from $\frac{k}{T}$. As an example case, the spectrogram of a family of *N* = 8 chirps is shown in Figure 8 in the case *T* = 1 ms.

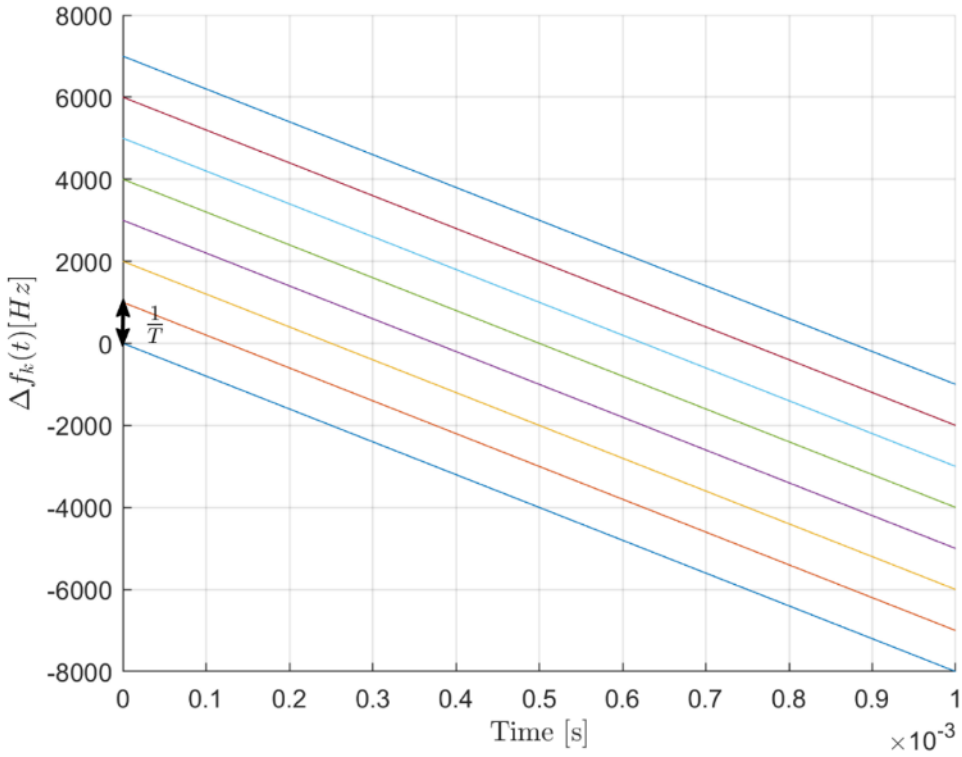

Figure 8: Frequency deviation. T = 1ms, N = 8, B = 8 KHz

As previously mentioned, the value *B* of the frequency sweep interval cannot be chosen independently of other modulation parameters, as it is related to the chirp-interval *T* and the number of chirps *N* by the following equation:

$$BT = N \tag{3.6}$$

In fact, the constraint posed by (3.6) is the basis for the generation and the demodulation of OCDM signals by means of numerical techniques, as well for their spectral characteristics. These issues will be discussed in the following sections.

3.2 Spectrum of the complex linear chirp

Let us compute $\Psi_k(f) = \mathcal{F}[\psi_k(t)g_T(t)] = \mathcal{F}[e^{j\frac{\pi}{4}}e^{-j\pi\frac{B}{T}\left(t-\frac{k}{B}\right)^2}g_T(t)]$. For the sake of simplicity, we will use the compact notation $\alpha = \frac{B}{T}$.

$$\Psi_k(f) = \mathcal{F}[e^{j\frac{\pi}{4}}e^{-j\pi\alpha\left(t-\frac{k}{B}\right)^2}g_T(t)]$$

$$= \int_{-\infty}^{\infty} e^{j\frac{\pi}{4}}e^{-j\pi\alpha\left(t-\frac{k}{B}\right)^2}g_T(t)\,e^{-j2\pi ft}dt$$

$$= e^{j\frac{\pi}{4}}\int_0^T e^{-j\pi\alpha\left(t-\frac{k}{B}\right)^2}e^{-j2\pi ft}dt.$$

By denoting $\left(t-\frac{k}{B}\right) = \eta$ it results

$$\Psi_k(f) = e^{j\frac{\pi}{4}}\int_{-\frac{k}{B}}^{T-\frac{k}{B}} e^{-j\pi\alpha\eta^2}\,e^{-j2\pi f(\eta+\frac{k}{B})}d\eta$$

$$= e^{j\frac{\pi}{4}}e^{-j2\pi f\frac{k}{B}}\int_{-\frac{k}{B}}^{T-\frac{k}{B}} e^{-j\pi[\alpha\eta^2+2f\eta]}\,d\eta$$

$$= e^{j\frac{\pi}{4}}e^{-j2\pi f\frac{k}{B}}\int_{-\frac{k}{B}}^{T-\frac{k}{B}} e^{-j\pi[\alpha\eta^2+2f\eta+\frac{f^2}{\alpha}]}e^{j\pi\frac{f^2}{\alpha}}\,d\eta$$

$$= e^{j\frac{\pi}{4}}e^{j\pi\frac{f^2}{\alpha}}e^{-j2\pi f\frac{k}{B}}\int_{-\frac{k}{B}}^{T-\frac{k}{B}} e^{-j\pi[\sqrt{\alpha}\eta+\frac{f}{\sqrt{\alpha}}]^2}\,d\eta.$$

By denoting $\sqrt{\alpha}\eta + \frac{f}{\sqrt{\alpha}} = \frac{\xi}{\sqrt{2}}$ it results

$$\Psi_k(f) = e^{j\frac{\pi}{4}} \frac{e^{j\pi\frac{f^2}{\alpha}} e^{-j2\pi f\frac{k}{B}}}{\sqrt{2\alpha}} \int_{\sqrt{2\alpha}\frac{k}{B}+\sqrt{\frac{2}{\alpha}}f}^{\sqrt{2\alpha}\left(T-\frac{k}{B}\right)+\sqrt{\frac{2}{\alpha}}f} e^{-j\frac{\pi}{2}\xi}\, d\xi$$

$$= e^{j\frac{\pi}{4}} \frac{e^{j\pi\frac{f^2}{\alpha}} e^{-j2\pi f\frac{k}{B}}}{\sqrt{2\alpha}} \int_{\sqrt{2\alpha}\frac{k}{B}+\sqrt{\frac{2}{\alpha}}f}^{\sqrt{2\alpha}\left(T-\frac{k}{B}\right)+\sqrt{\frac{2}{\alpha}}f} \cos\left(\frac{\pi}{2}\xi^2\right) - \mathrm{j}\sin(\frac{\pi}{2}\xi^2)\, d\xi$$

$$= e^{j\frac{\pi}{4}} \frac{e^{j\pi\frac{f^2}{\alpha}} e^{-j2\pi f\frac{k}{B}}}{\sqrt{2\alpha}} \left[\int_{\sqrt{2\alpha}\frac{k}{B}+\sqrt{\frac{2}{\alpha}}f}^{\sqrt{2\alpha}\left(T-\frac{k}{B}\right)+\sqrt{\frac{2}{\alpha}}f} \cos\left(\frac{\pi}{2}\xi^2\right) d\xi - j \int_{\sqrt{2\alpha}\frac{k}{B}+\sqrt{\frac{2}{\alpha}}f}^{\sqrt{2\alpha}\left(T-\frac{k}{B}\right)+\sqrt{\frac{2}{\alpha}}f} \sin(\frac{\pi}{2}\xi^2) d\xi \right]$$

$$= e^{j\frac{\pi}{4}} \frac{e^{j\pi\frac{f^2}{\alpha}} e^{-j2\pi f\frac{k}{B}}}{\sqrt{2\alpha}} \left[\int_0^{\sqrt{2\alpha}\left(T-\frac{k}{B}\right)+\sqrt{\frac{2}{\alpha}}f} \cos\left(\frac{\pi}{2}\xi^2\right) d\xi - \int_0^{-\sqrt{2\alpha}\frac{k}{B}+\sqrt{\frac{2}{\alpha}}f} \cos\left(\frac{\pi}{2}\xi^2\right) d\xi - \right.$$

$$\left. -j \int_0^{\sqrt{2\alpha}\left(T-\frac{k}{B}\right)+\sqrt{\frac{2}{\alpha}}f} \sin\left(\frac{\pi}{2}\xi^2\right) d\xi + j \int_0^{-\sqrt{2\alpha}\frac{k}{B}+\sqrt{\frac{2}{\alpha}}f} \sin\left(\frac{\pi}{2}\xi^2\right) d\xi \right]$$

$$= e^{j\frac{\pi}{4}} \frac{e^{j\pi\frac{f^2}{\alpha}} e^{-j2\pi f\frac{k}{B}}}{\sqrt{2\alpha}} \left[C(\sqrt{2\alpha}\left(T-\frac{k}{B}\right) + \sqrt{\frac{2}{\alpha}}f) - C(-\sqrt{2\alpha}\frac{k}{B} + \sqrt{\frac{2}{\alpha}}f) - \right.$$

$$\left. - jS(\sqrt{2\alpha}\left(T-\frac{k}{B}\right) + \sqrt{\frac{2}{\alpha}}f) + jS(-\sqrt{2\alpha}\frac{k}{B} + \sqrt{\frac{2}{\alpha}}f) \right], \qquad (3.7)$$

where $S(x) \triangleq \int_0^x \sin\left(\frac{\pi}{2}t^2\right) dt$ and $C(x) \triangleq \int_0^x \cos\left(\frac{\pi}{2}t^2\right) dt$ are the Fresnel integrals.

As an example case, Figure 9 shows $|\Psi_k(f)|$, that is, the amplitude spectrum of $\psi_k(t)g_T(t)$, for k = 0 (leftmost plot) and k = 1023 (rightmost plot) in the case N = 1024, B = 5GHz and, consequently, $T = \frac{N}{B} = 2.048 \cdot 10^{-7}\ s$. For intermediate values of k, the spectra of the corresponding chirps fall between the two extreme cases represented in the figure.

It is worth observing that, when all are considered, the N chirps of an OCDM signal span a frequency interval of width 2B.

3.3 Discrete-time OCDM signal

Let us focus the attention on the complex envelope of OCDM signals in the generic *n*th chirp-interval:

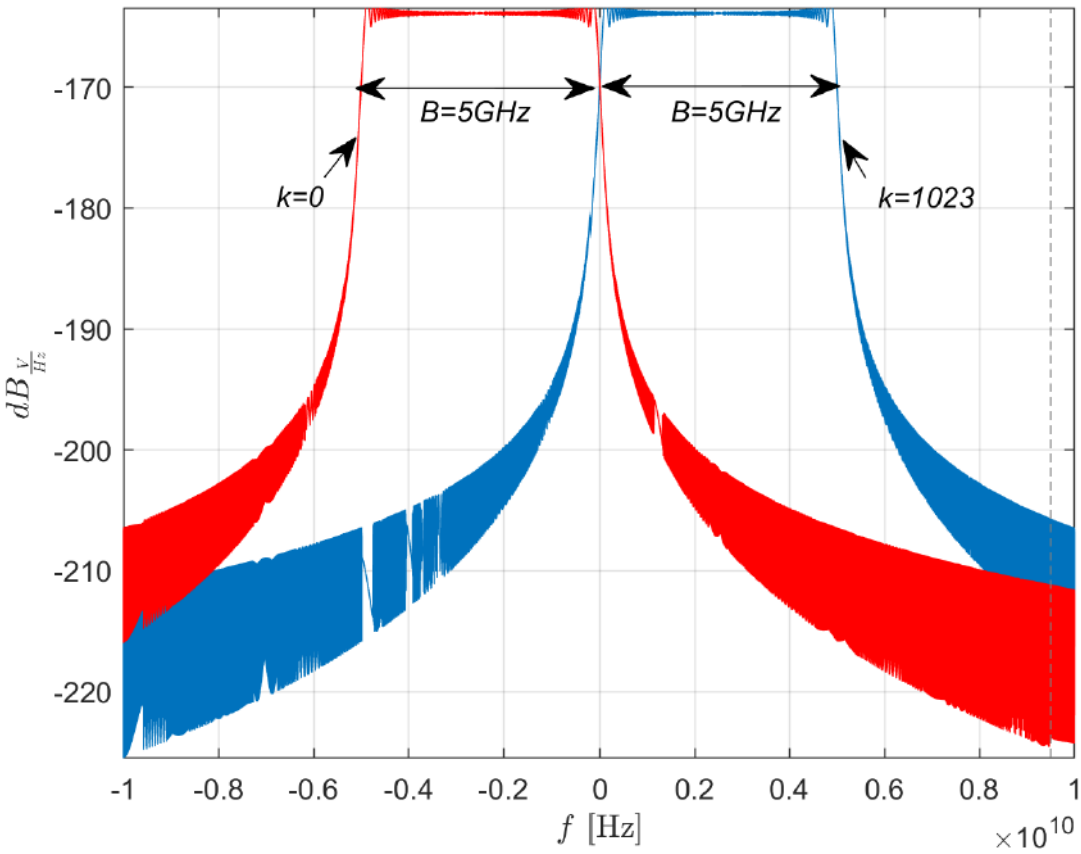

Figure 9: Chirp spectra for k = 0 (leftmost plot) and k = 1023 (rightmost plot). B = 5 GHz, T =2.048 ·10^{-7}, N = 1024.

$$i_n(t) = \sum_{k=0}^{N-1} x_k(n)\, e^{j\frac{\pi}{4}} e^{-j\pi\frac{B}{T}\left(t-nT-\frac{k}{B}\right)^2} g_t(t-nT) \tag{3.8}$$

Without loss of generality, in order to ease the notation, we consider the expression (3.8) for $n = 0$, thus assuming $[0\ T]$ as reference chirp-interval, also denoting $x_k(0) = x_k$ for the sake of compactness:

$$i_0(t) = \sum_{k=0}^{N-1} x_k\, e^{j\frac{\pi}{4}} e^{-j\pi\frac{B}{T}\left(t-\frac{k}{B}\right)^2} g_t(t) \tag{3.9}$$

Taking *N* samples of (3.9) spaced by T_s in the reference interval [0 *T*], which means assuming a sampling rate $f_s = \frac{1}{T_S} = \frac{N}{T}$ and sampling instants $t_m = mT_s$ $(m = 0, 1, \dots N-1)$, yields:

$$i_0(t_m) = \sum_{k=0}^{N-1} x_k \, e^{j\frac{\pi}{4}} e^{-j\pi\frac{B}{T}\left(t_m - \frac{k}{B}\right)^2} g_t(t_m)$$

$$= \sum_{k=0}^{N-1} x_k \, e^{j\frac{\pi}{4}} e^{-j\pi\frac{B}{T}\left(m\frac{T}{N} - \frac{k}{B}\right)^2} g_t\left(m\frac{T}{N}\right)$$

$$= e^{j\frac{\pi}{4}} \sum_{k=0}^{N-1} x_k \, e^{-j\pi\frac{B}{T}\frac{T^2}{N^2}\left(m - \frac{k}{B}\frac{N}{T}\right)^2} g_t\left(m\frac{T}{N}\right) \text{ with } m = 0, 1, \dots, N-1 \qquad (3.10)$$

By recalling (3.6), (3.10) can be further elaborated as

$$i_0(t_m) = e^{j\frac{\pi}{4}} \sum_{k=0}^{N-1} x_k \, e^{-j\frac{\pi}{N}(m-k)^2} g_t\left(m\frac{T}{N}\right) \text{ with } m = 0, 1, \dots, N-1. \qquad (3.11)$$

Given the definition of $g_T(t)$, the samples of the complex envelope in the considered chirp-interval can be finally expressed as:

$$i_0(t_m) = e^{j\frac{\pi}{4}} \sum_{k=0}^{N-1} x_k \, e^{-j\frac{\pi}{N}(m-k)^2} \text{ with } m = 0, 1, \dots, N-1. \qquad (3.12)$$

Remarkably, (3.12) is also the definition of the inverse discrete Fresnel transform (IDFnT), thus showing that the latter is the straightforward mathematical tool for the generation of discrete time OCDM signals.

3.4 Received signal in the presence of phase noise

Let us rewrite (3.12), simplifying the notation:

$$i_m = i_0(t_m) = e^{j\frac{\pi}{4}} \sum_{k=0}^{N-1} x_k \, e^{-j\frac{\pi}{N}(m-k)^2} \quad \text{with } m = 0, 1, \dots, N-1. \qquad (3.13)$$

The *m*-th sample of the received signal is

$$r_m = (i_m + w_m) e^{j\phi_m} \text{ with } m = 0, 1, \dots, N-1, \qquad (3.14)$$

where $w_m \sim \mathbb{C}\mathcal{N}(0, \sigma_N^2)$. A complex Gaussian random variable is insensitive to rotations, so the complex Gaussian noise under phase noise has the same statistic of the complex Gaussian noise:

$$w_m e^{j\phi_m} \sim w_m, \tag{3.15}$$

thus we can write

$$r_m = i_m\, e^{j\phi_m} + w_m \text{ with } m = 0, 1, \dots, N-1. \tag{3.16}$$

That is the analogous of (2.13) for a multicarrier modulation: we are considering a frequency flat channel affected by white noise and phase noise. At the receiver, a Discrete Fresnel Transform (DFnT) is performed, in order to demodulate the transmitted signal (3.13), that it has been modulated through a IDFnT. A normalization is also performed:

$$y_l = \frac{1}{N}\sum_{m=0}^{N-1} r_m e^{-j\frac{\pi}{4}}\, e^{j\frac{\pi}{N}(l-m)^2} \quad \text{with } l = 0, 1, \dots, N-1. \tag{3.17}$$

By substituting (3.16) in (3.17) we obtain

$$y_l = \frac{1}{N}\sum_{m=0}^{N-1} \left(i_m\, e^{j\phi_m} + w_m\right) e^{-j\frac{\pi}{4}}\, e^{j\frac{\pi}{N}(l-m)^2} \text{ with } l = 0, 1, \dots, N-1, \tag{3.18}$$

and by substituting (3.13) in (3.18) we obtain

$$y_l = \frac{1}{N}\sum_{m=0}^{N-1} \left(e^{j\frac{\pi}{4}} \sum_{k=0}^{N-1} x_k\, e^{-j\frac{\pi}{N}(m-k)^2} e^{j\phi_m} + w_m \right) e^{-j\frac{\pi}{4}}\, e^{j\frac{\pi}{N}(l-m)^2} \tag{3.19}$$

$$\text{with } l = 0, 1, \dots, N-1$$

which can be manipulated as follow:

$$y_l = \frac{1}{N}\sum_{m=0}^{N-1} e^{j\frac{\pi}{4}} \sum_{k=0}^{N-1} x_k\, e^{-j\frac{\pi}{N}(m-k)^2} e^{j\phi_m} e^{-j\frac{\pi}{4}}\, e^{j\frac{\pi}{N}(l-m)^2} + \frac{1}{N}\sum_{m=0}^{N-1} w_m e^{-j\frac{\pi}{4}}\, e^{j\frac{\pi}{N}(l-m)^2}.$$

By considering that a complex Gaussian random variable is insensitive to rotations, as we did previously, we can simplify as follow:

$$y_l = \frac{1}{N}\sum_{m=0}^{N-1} e^{j\frac{\pi}{4}} \sum_{k=0}^{N-1} x_k\, e^{-j\frac{\pi}{N}(m-k)^2} e^{j\phi_m} e^{-j\frac{\pi}{4}} e^{j\frac{\pi}{N}(l-m)^2} + \frac{1}{N}\sum_{m=0}^{N-1} w_m$$

$$= \frac{1}{N}\sum_{m=0}^{N-1} x_l e^{-j\frac{\pi}{N}(m-l)^2} e^{j\phi_m}\, e^{j\frac{\pi}{N}(l-m)^2} + \frac{1}{N}\sum_{m=0}^{N-1}\sum_{\substack{k=0 \\ k\neq l}}^{N-1} x_k\, e^{-j\frac{\pi}{N}(m-k)^2} e^{j\phi_m}\, e^{j\frac{\pi}{N}(l-m)^2} + \frac{1}{N}\sum_{m=0}^{N-1} w_m$$

$$= x_l \frac{1}{N}\sum_{m=0}^{N-1} e^{j\phi_m} + \frac{1}{N}\sum_{\substack{k=0 \\ k\neq l}}^{N-1} x_k \sum_{m=0}^{N-1} e^{j\phi_m}\, e^{-j\frac{\pi}{N}(k-l)(k+l-2m)} + \frac{1}{N}\sum_{m=0}^{N-1} w_m \qquad (3.20)$$

$$\text{with } l = 0, 1, \dots, N-1$$

Two important components have been highlighted, that can be named similarly to the ones that it is possible to find, with a similar procedure, in OFDM [29]: the Common Phase Error (CPE) and the Inter-Chirp Interference (ICI).

$$\text{CPE} = x_l \frac{1}{N}\sum_{m=0}^{N-1} e^{j\phi_m} \qquad (3.21)$$

$$\text{ICI} = \frac{1}{N}\sum_{\substack{k=0 \\ k\neq l}}^{N-1} x_k \sum_{m=0}^{N-1} e^{j\phi_m}\, e^{-j\frac{\pi}{N}(k-l)(k+l-2m)} \qquad (3.22)$$

CPE affects each chirp in the same way, while the ICI effect depends on the chirp.

3.5 Compensation of the Common Phase Error (CPE)

As previously said, CPE affects each chirp in the same way: this phenomenon occurs also in OFDM systems affected by phase noise, and several compensation schemes have been developed. In this thesis the compensation scheme presented in [30] has been used.

The compensation works as follow: for each OCDM symbol, each chirp is affected by the same CPE. We try to estimate each symbol y_l to which constellation point corresponds. In our system, we can have errors due to phase noise and AWGN noise, so it is possible to have a wrong association. Let us call the estimated constellation point $\tilde{y}_l$: now we compute the

average phase shift of each symbol with respect to the corresponding estimated constellation point, that is an estimate of CPE

$$\hat{\phi}_{\mathrm{CPE}} = \frac{1}{N}\sum_{l=0}^{N-1} \angle y_l - \angle \tilde{y}_l. \tag{3.23}$$

Now we are able to update the received symbol by compensating the CPE with its estimation: instead of performing the estimation on y_l, now we do it on

$$y_l e^{-\hat{\phi}_{\mathrm{CPE}}}. \tag{3.24}$$

4. Numerical Results

In Chapter 2 phase noise has been characterized and in Chapter 3 OCDM has been described: now it is possible to simulate a THz communication system impaired by phase noise and white noise (superposition of thermal noise and molecular noise).

First of all, it is necessary to determine which is the amount of phase noise present in the system, which means that we have to decide which oscillator is used in that system. In other words, we have to find the parameters of (2.20).

As said previously, THz communications components could be realized using electronics or photonics technologies. Using electronic technologies, the signal is upconverted to THz frequency, while in optical case the signal is downconverted. Let us see two oscillators realized with these two different technologies: in [31], a 560 GHz frequency synthesizer realized in CMOS technology is presented, whereas in [32] a 300 GHz oscillator realized in photonic technology is presented. In the following figures their phase noise is measured.

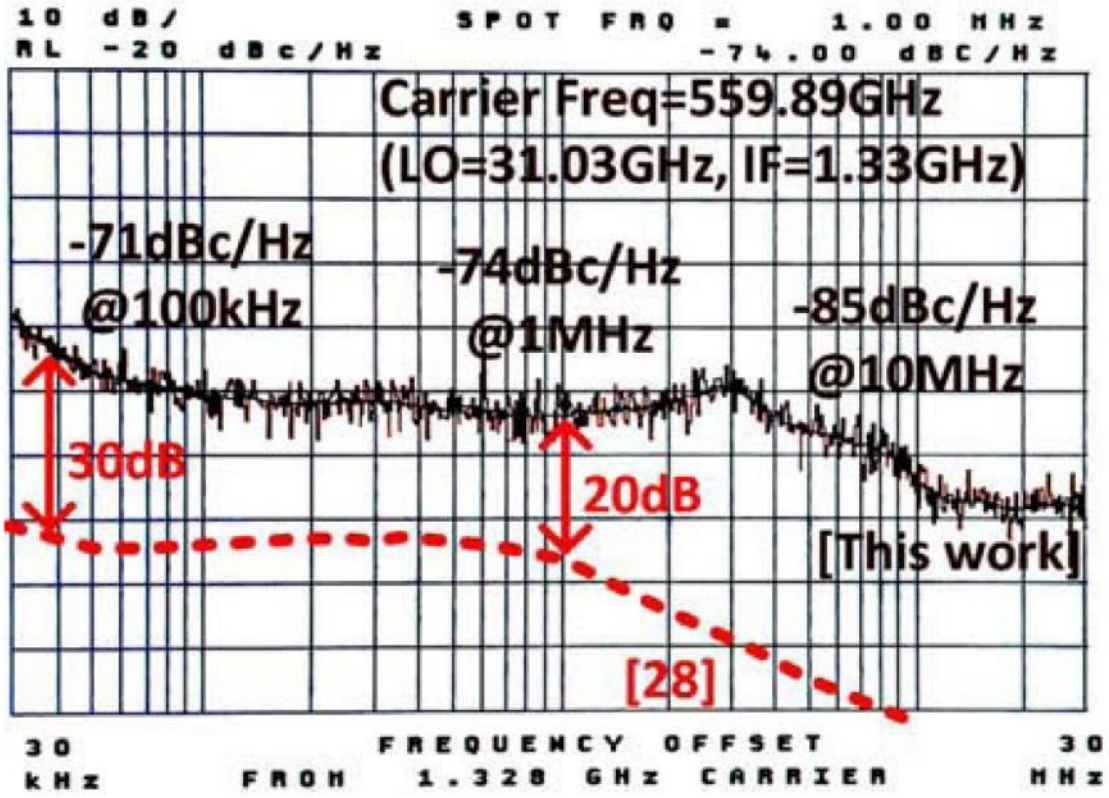

Figure 10: Phase noise measurement of the 559.89 GHz tone of the frequency synthesizer realized in CMOS technology [31]

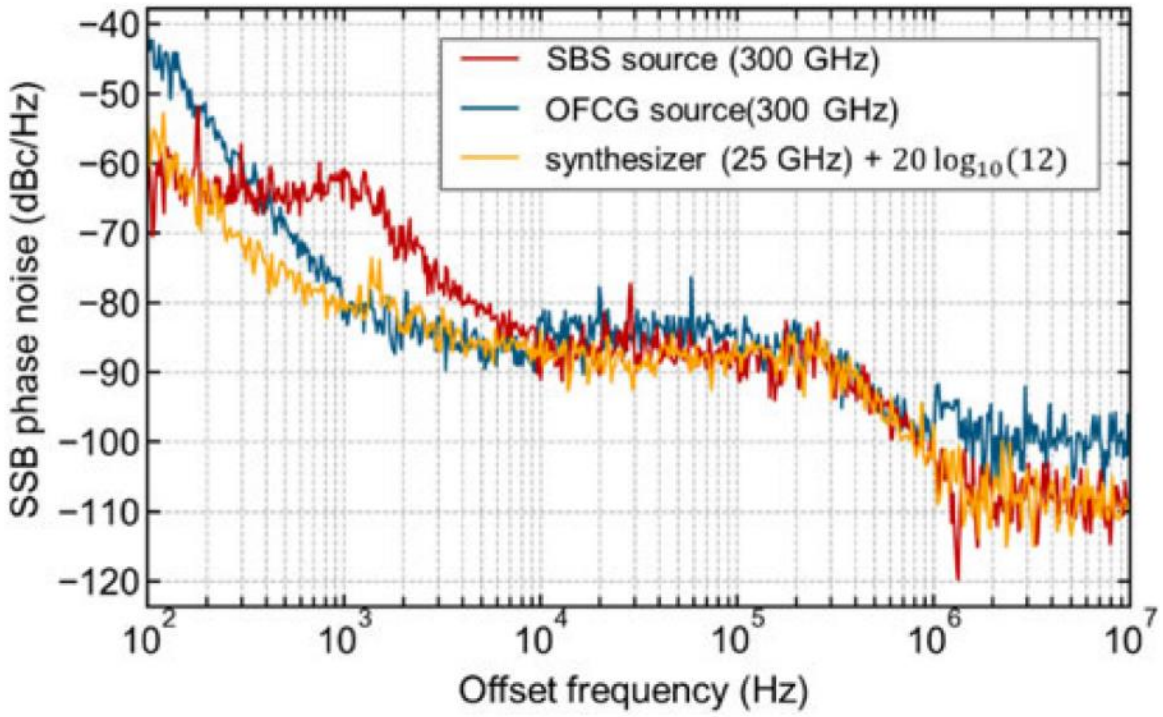

Figure 11: Phase noise measurement of the SBS-based source at 300 GHz (realized with optical technology) [32]

Phase noise in the 560 GHz oscillator is much higher than the one of the 300 GHz optical source. This is the reason why we take into account the parameters that come from the second oscillator, the optical one.

As we can see in Figure 11, the corner frequency f_c is about 1 MHz, and K_0 is about -110 dBc. Using (2.20), it is possible to obtain K_2: now all the parameters needed to simulate phase noise are available. Observing (2.19), we can see that we also need *T*, and we also need *B* in order to simulate the white component of the phase noise. Considering (3.6), those two parameters are related through *N*, the number of orthogonal chirps. *B* has been considered in the order of GHz, since the huge bandwidth is one of the main advantages of THz communications.

The first simulation has been carried out considering $f_c = 1\,MHz$, $K_0 = -110\,dBc$, $B = 10\,GHz$, and N is a parameter that is changed, assuming in particular $N \in \{128, 512, 1024, 2048\}$.

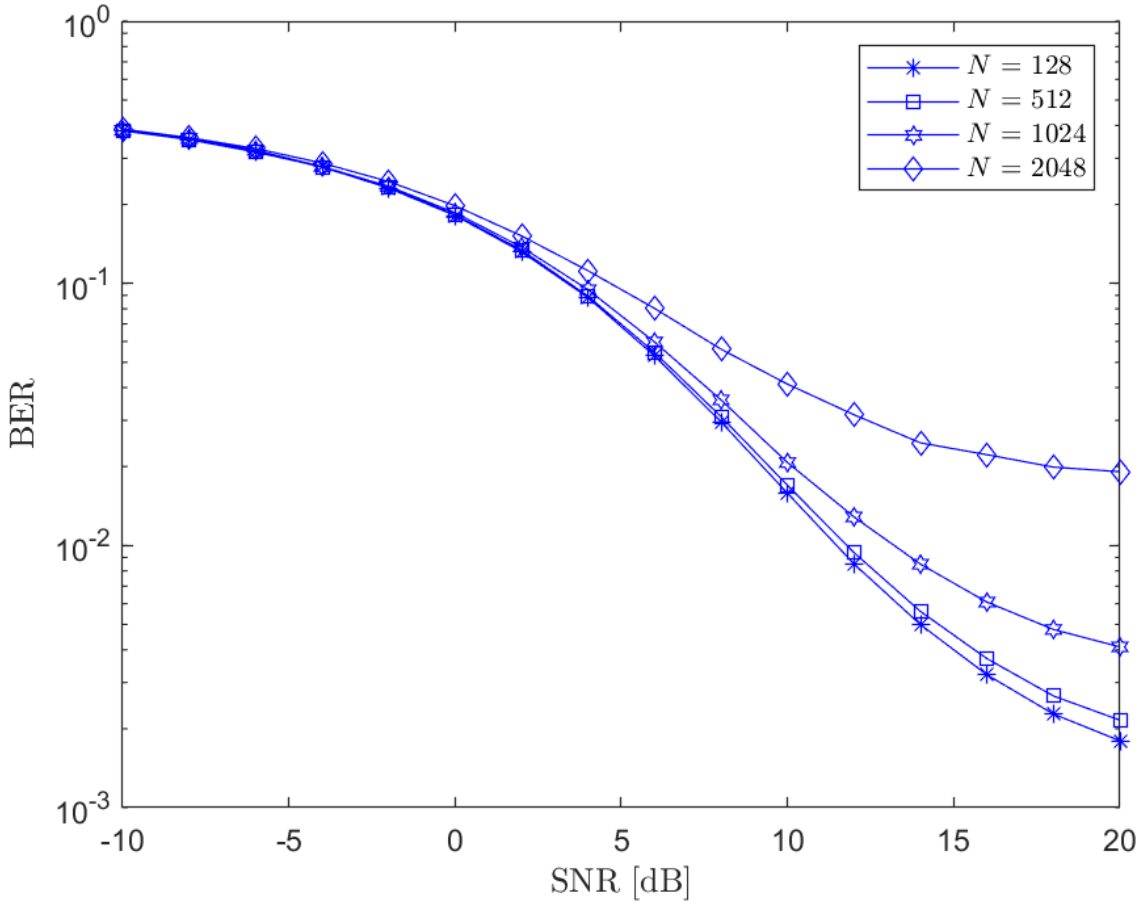

Figure 12: BER *vs* SNR. f_c = *1 MHz,* K_0 = *-110 dBc, B = 10 GHz, N = 128, 512, 1024, 2048.*

In Figure 12, which shows the bit error rate (BER) as a function of the signal to noise ratio (SNR), we can see that the performance depends on *N*. In particular the greater is *N*, the worse are the performance. SNR is defined as the average power of the useful signal divided by the power of noise. It is also possible to see that a performance floor is present, due to phase noise: after a certain level of SNR, it is useless trying to improve BER by increasing it.

This phenomenon can be explained intuitively by considering Figure 8, in which we can see the frequency deviation of $N = 8$ chirps, and the spacing in frequency between different chirps is $\frac{1}{T}$. By manipulating (3.6) we obtain

$$\frac{1}{T} = \frac{B}{N}. \tag{4.1}$$

If *B* is fixed, by increasing *N* we reduce the frequency spacing between chirps, and so, due to phase noise, the higher is *N*, the higher is the probability that they interfere each other.

The second simulation has been carried considering the very same parameters of the first one, but phase noise has been changed: we considered only white noise, neglecting the Wiener component.

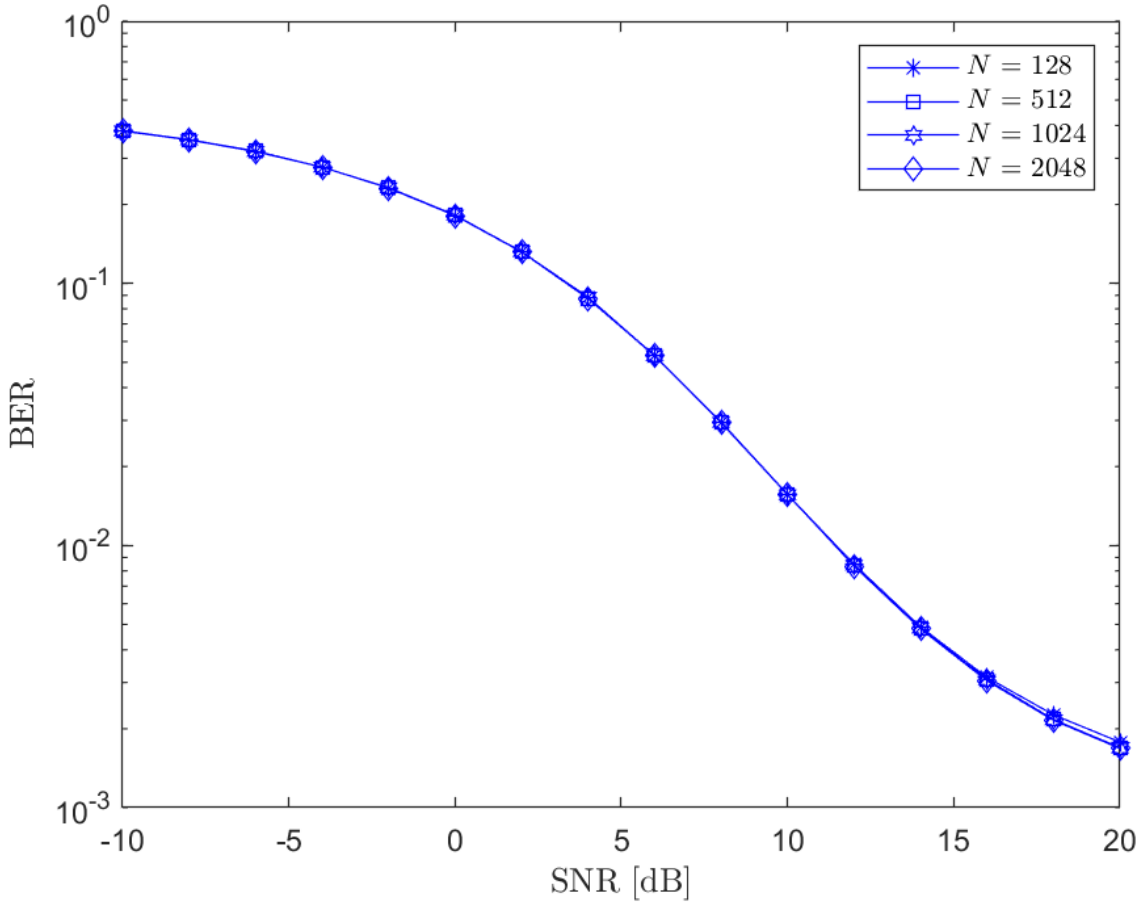

Figure 13: BER *vs* SNR. f_c *= 1 MHz,* K_0 *= -110 dBc, B = 10 GHz, N = 128, 512, 1024, 2048. Phase noise only white, Wiener component has been neglected.*

In Figure 13, we can see that if we consider only the white component of phase noise, performance does not depend on *N*, and this shows that this model is not accurate enough. The different behaviour with respect to the first simulation is due to the phase noise statistics: its sample are Gaussian and uncorrelated, so the phase noise does not depend on the number of samples, and this leads to a common error for each chirp. This means that each chirp is translated of the same quantity, and they do not interfere each other.

Since this simulation proved that considering only the white phase noise provides inaccurate results, all the next simulations will be carried out considering both white and Wiener components.

The third simulation investigated the behaviour of the system when changing K_0, that is, the level of the white noise floor. The parameters are $f_c = 1\ MHz$, $N = 1024$, $B = 10\ GHz$, and K_0 has been changed, assuming in particular $K_0 = -110\ dBc, -120\ dBc, -130\ dBc$.

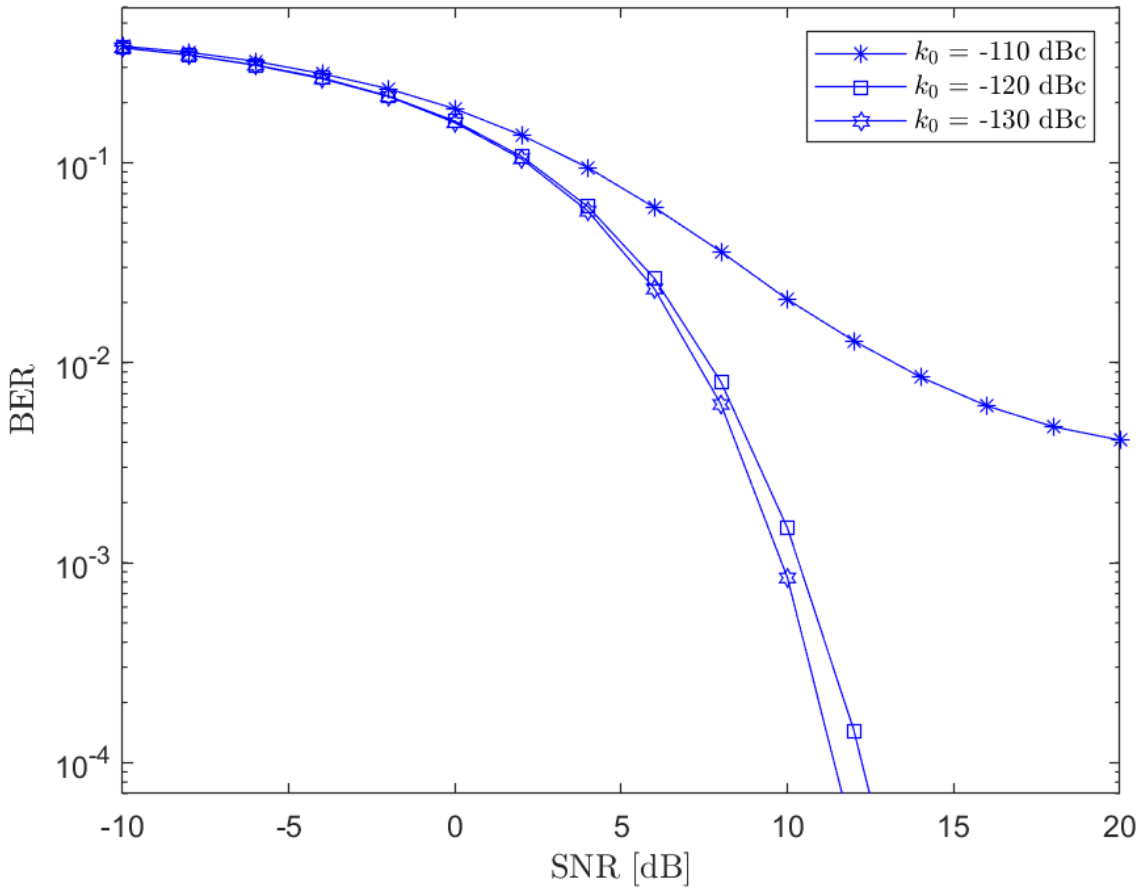

Figure 14: BER *vs* SNR. f_c = *1 MHz, B = 10 GHz, N = 1024,* K_0 = *-110 dBc, -120 dBc, -130 dBc.*

As we can see in Figure 14, the performance floor due to phase noise is clearly evident when K_0 = -110 dBc, while with the others two values the performance floor is below the BER interval shown in the figure. Values of K_0 higher than -110 dBc have not been considered, because they would have led to too much high value of BER.

As we can see, if oscillators technology improves, we would be able to have excellent performance. It seems that only photonics oscillators will be able to provide a signal good enough to enable next generation communications, since the nature of electronics oscillators lead to a too much strong phase noise.

The fourth simulation investigated what happens if the corner frequency f_c changes. The parameters are $K_0 = -110\ dBc$, $B = 10\ GHz$, $N = 1024$, and $f_c = 100\ kHz$, $1\ MHz$, $10\ MHz$.

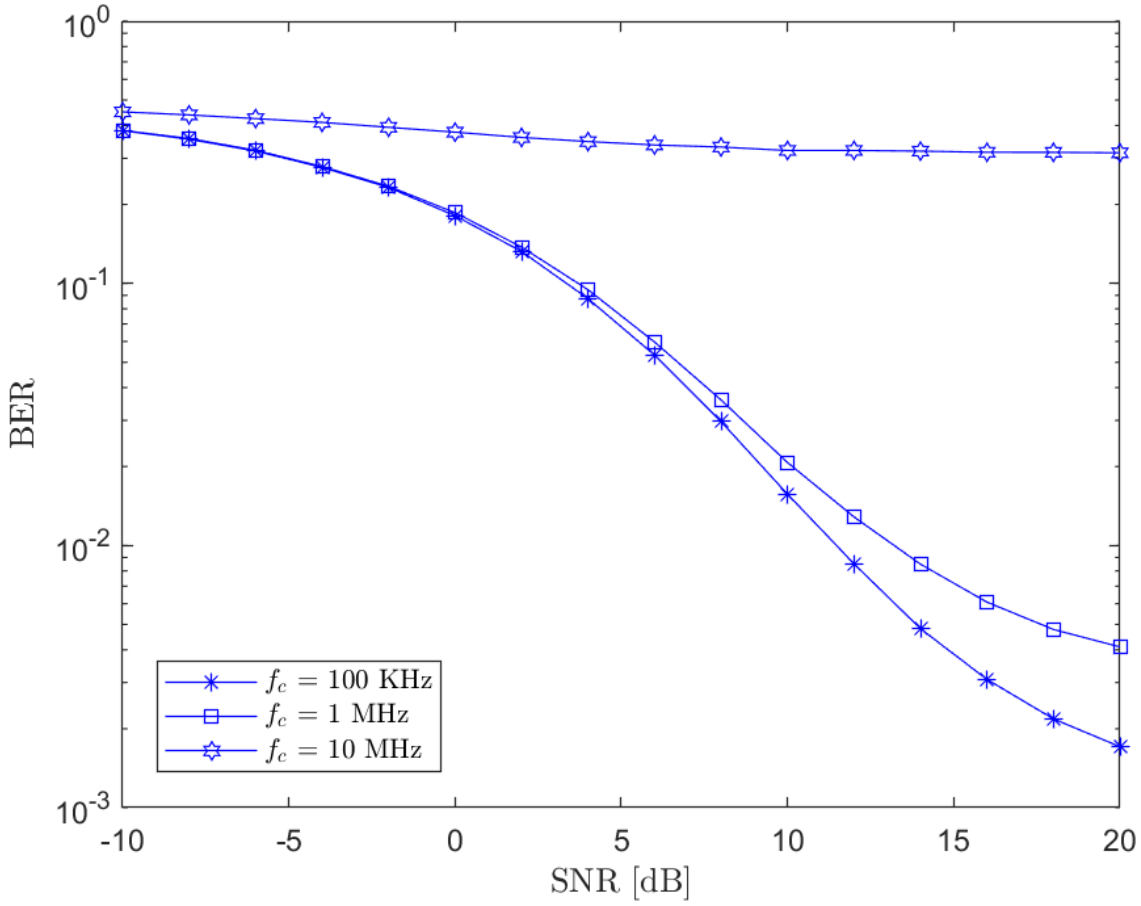

Figure 15: BER *vs* SNR. *K_0 = -110 dBc, B = 10 GHz, N = 1024, f_c = 100 KHz, 1 MHz, 10 MHz.*

In Figure 15 we can see that with $f_c = 10\ MHz$, the system does not work, while with $f_c = 100\ KHz$ the performance level is reasonable.

In the fifth simulation the impact of B on the system behaviour was investigated. The parameters are $f_c = 1\ MHz$, $K_0 = -110\ dBc$, $N = 1024$, and *B = 500 MHz, 1 GHz, 5 GHz, 10 GHz, 20 GHz.*

In Figure 16 we can see the results, which shows that there is an optimum value: the green curve, the one corresponding to B = 5 GHz, is the one that provides the best performance.

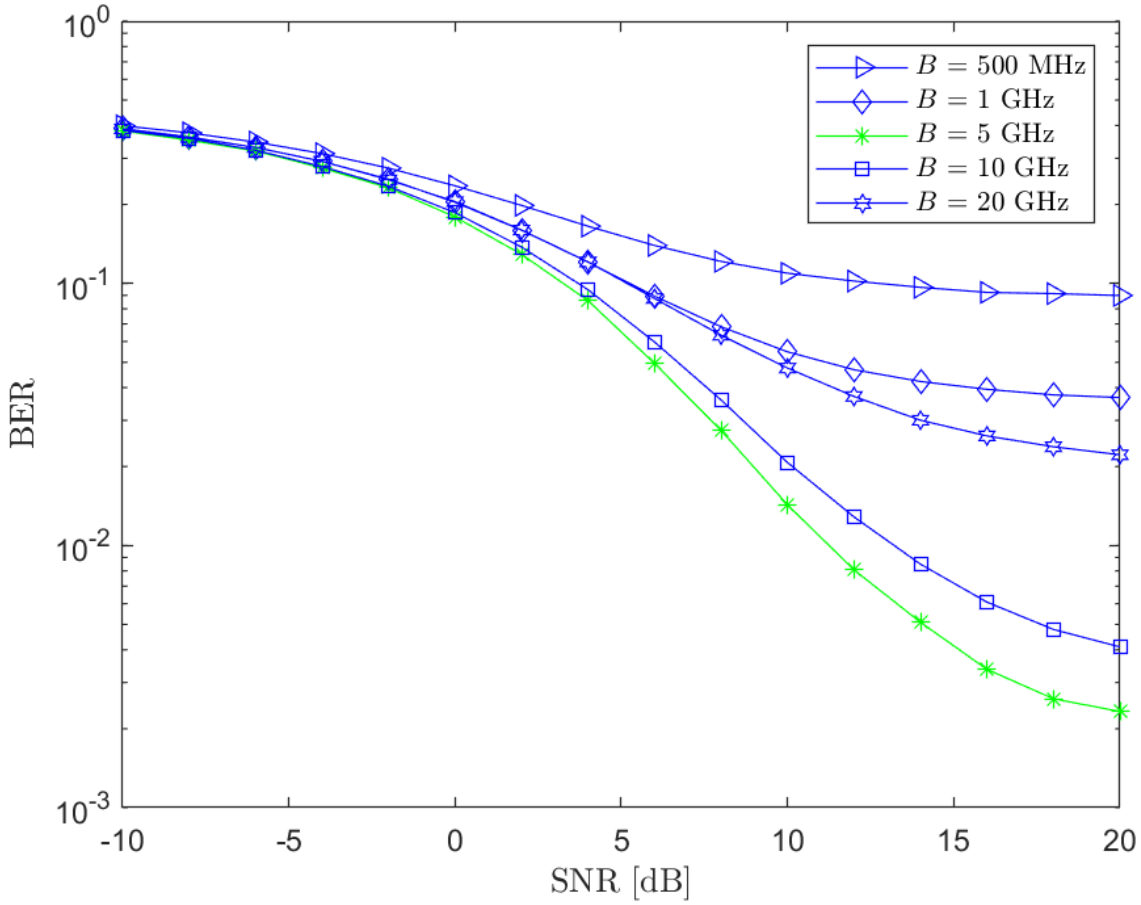

Figure 16: BER *vs* SNR. f_c*=1 MHz,* K_0*= -110 dBc, N = 1024, and B = 500 MHz, 1 GHz, 5 GHz, 10 GHz, 20 GHz.*

As previously highlighted when discussing the results of Simulation 1, if we increase *N*, while keeping *B* fixed, the frequency spacing between chirps is reduced, and the system shows worse performance. According to (4.1), we obtain the same result when *N* is fixed and *B* decreases, so it is clear why *B = 500 MHz* and *B = 1 GHz* perform worse with respect to *B = 5 GHz*. The reason why *B = 10 GHz* and *B = 20 GHz* perform worse is because, even if the spacing between chirps is larger, the standard deviation of phase noise increases in such a way that it overcomes the benefit of a bigger spacing between chirps. This means that there is a trade-off between chirp compression and amount of phase noise in the system.

In order to better understand this phenomenon, a further simulation, the sixth, has been carried out: SNR has been fixed ($\text{SNR} = 15\ dB$) and then BER has been computed as a function of *B*. The parameters are $f_c = 1\ MHz$, $K_0 = -110\ dBc$, $\text{SNR} = 15\ dB$, $N = 256,\ 512,\ 1024$.

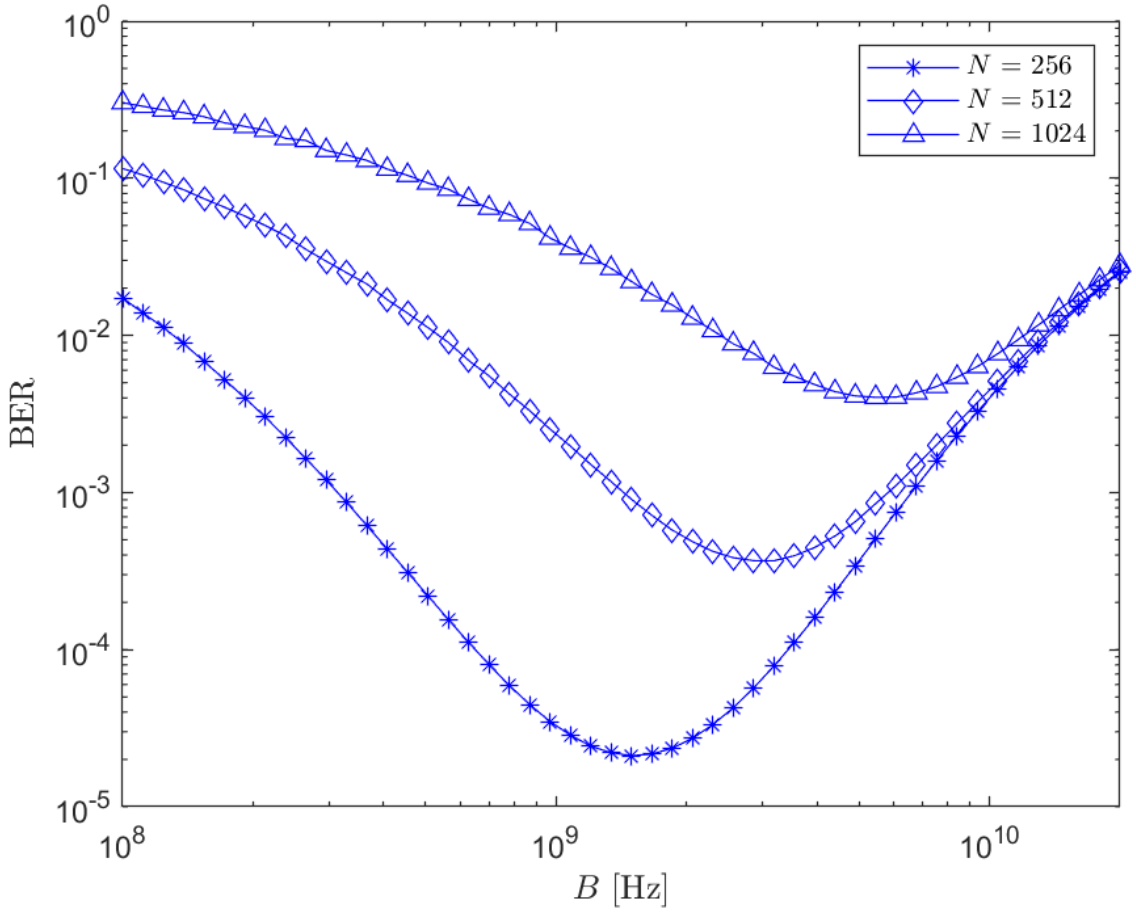

Figure 17: BER *vs B.* f_c*=1 MHz,* K_0*= -110 dBc,* SNR *= 15 dB and N = 256, 512, 1024.*

As we can see in Figure 17, the aforementioned optimum values are clearly visible, and they depend on *N*. The lower is *N*, the lower is the value of *B* that provides the optimum value. The next simulations aim to find if the optimum values found previously depends on the SNR.

In Figure 18 there are the results of the seventh simulation, in which BER has been computed as a function of *B*, and with parameters $f_c = 1\ MHz$, $K_0 = -110\ dBc$, SNR $= 10\ dB$, $N = 256,\ 512,\ 1024$. There are also the curves of the sixth simulation. As we can see, the optimum values change with SNR, and in order to better highlight this phenomenon, other two simulations have been carried: in the eighth simulation, the system has been simulated with parameters $f_c = 1\ MHz$, $K_0 = -110\ dBc$, SNR $= 5\ dB, 10\ dB, 15\ dB$, $N = 256$ (Figure 19), in the ninth simulation, the system has been simulated with parameters $f_c = 1\ MHz$, $K_0 = -110\ dBc$, SNR $= 5\ dB, 10\ dB, 15\ dB$, $N = 1024$ (Figure 20).

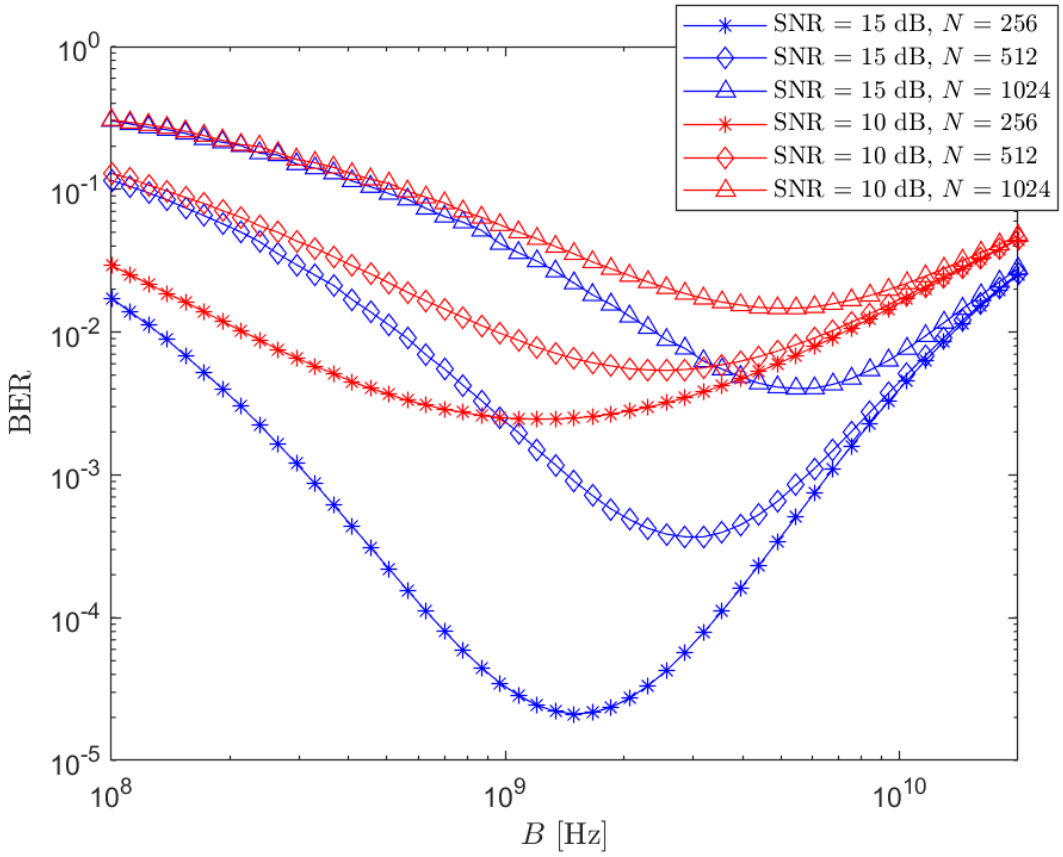

Figure 18: BER *vs B.* f_c*=1 MHz,* K_0*= -110 dBc,* SNR *= 10 dB, 15 dB, and N = 256, 512, 1024.*

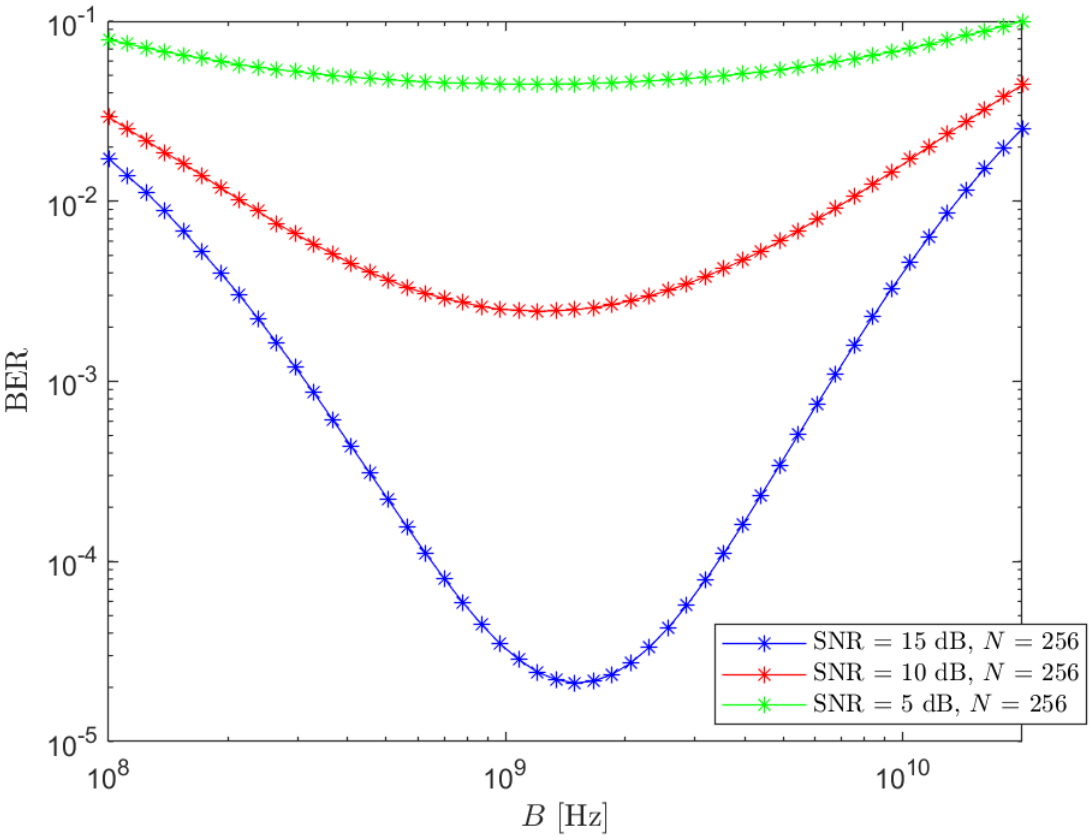

Figure 19: BER *vs B.* f_c*=1 MHz,* K_0*= -110 dBc,* SNR *= 5 dB, 10 dB, 15 dB and N = 256.*

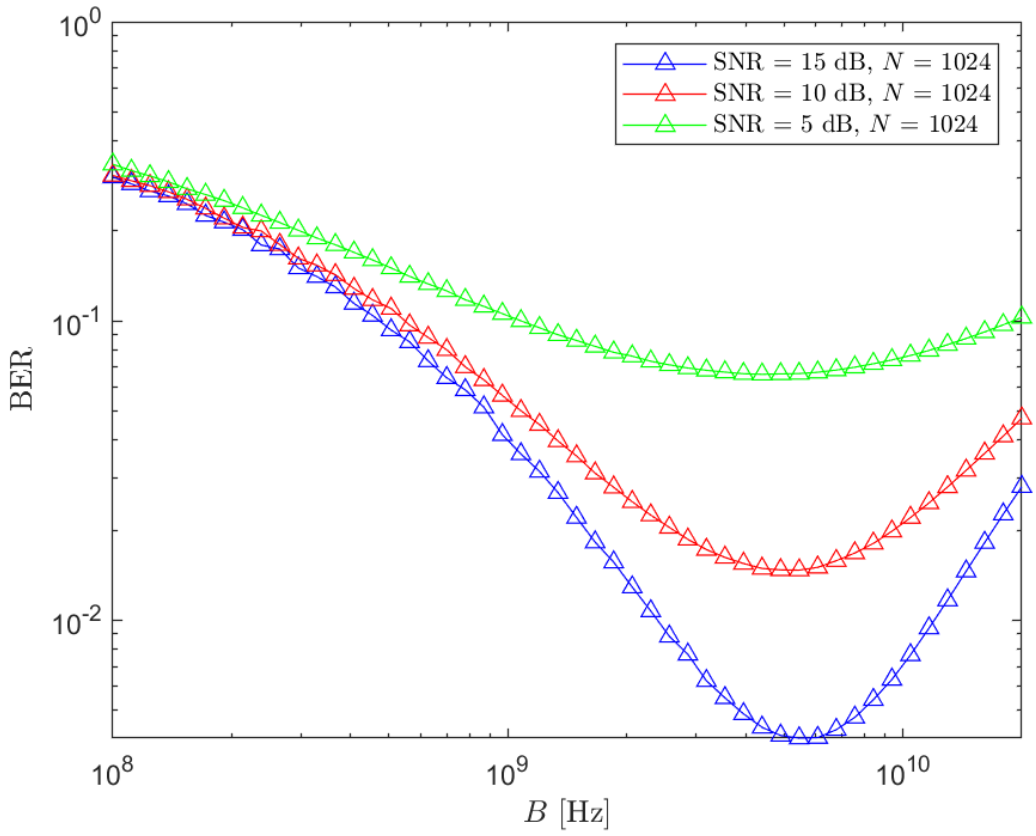

Figure 20: BER *vs B.* f_c*=1 MHz,* K_0*= -110 dBc,* SNR *= 5 dB, 10 dB, 15 dB and N = 1024.*

4.1 Numerical results after CPE compensation

The compensation algorithm introduced in the subchapter 3.5 could certainly improve the performance of the system, so additional simulations have been performed. In the tenth simulation the same parameters of the first one have been considered: $f_c = 1\ MHz$, $K_0 = -110\ dBc$, $B = 10\ GHz$, $N \in \{128, 512, 1024, 2048\}$, but now the compensation is applied. In Figure 21, which shows the BER as a function of the SNR, the results are shown, together with the ones without compensation: as it is possible to see, the CPE compensation algorithm works. The reduction of the BER when N = 2048 is significant: when SNR = 20 dB, it passes from 0.0191 to 0.0084; on the opposite, when N = 128, the improvement is almost negligible: BER, with SNR = 20 dB, passes from 0.00180 to 0.00173.

As we saw in the sixth simulation (and in Figure 17), performances depend on B: this suggested us to carry an analogous simulation, the eleventh, in which the CPE is compensated. SNR has been fixed ($\text{SNR} = 15\ dB$) and then BER has been computed as a function of B. The parameters are $f_c = 1\ MHz$, $K_0 = -110\ dBc$, $\text{SNR} = 15\ dB$, $N = 256,\ 512,\ 1024$.

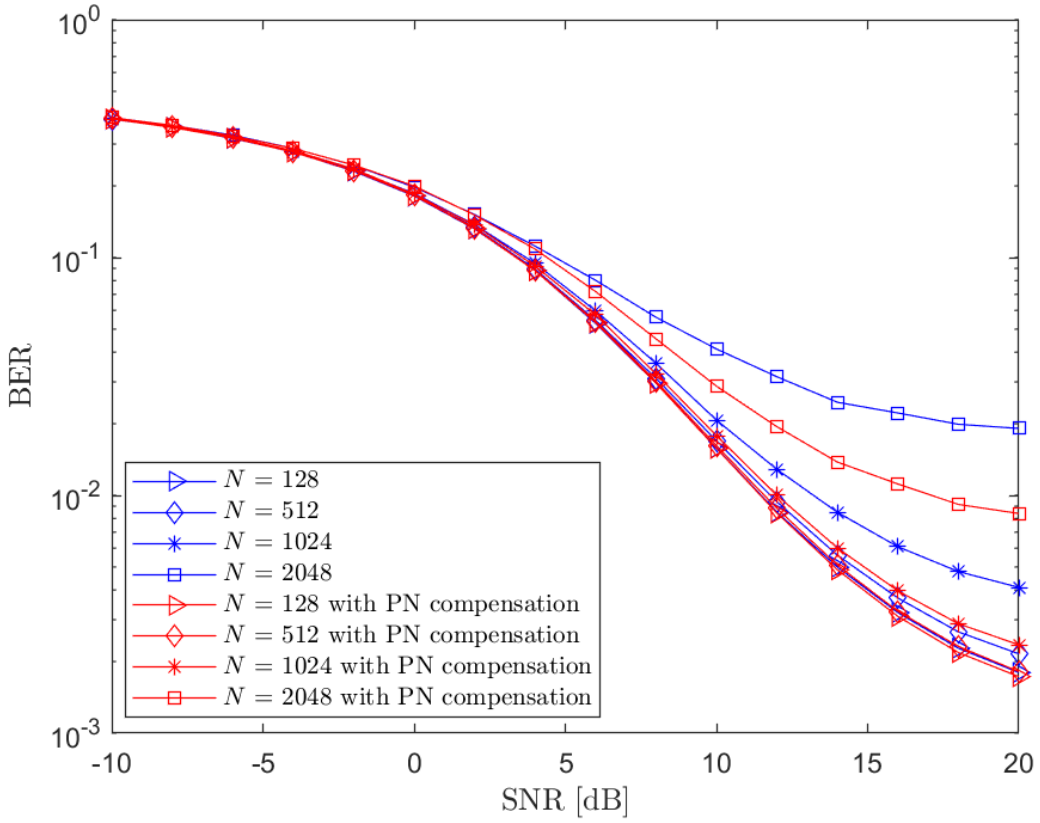

Figure 21: BER vs SNR. f_c *= 1 MHz,* K_0 *= -110 dBc, B = 10 GHz, N = 128, 512, 1024, 2048.*

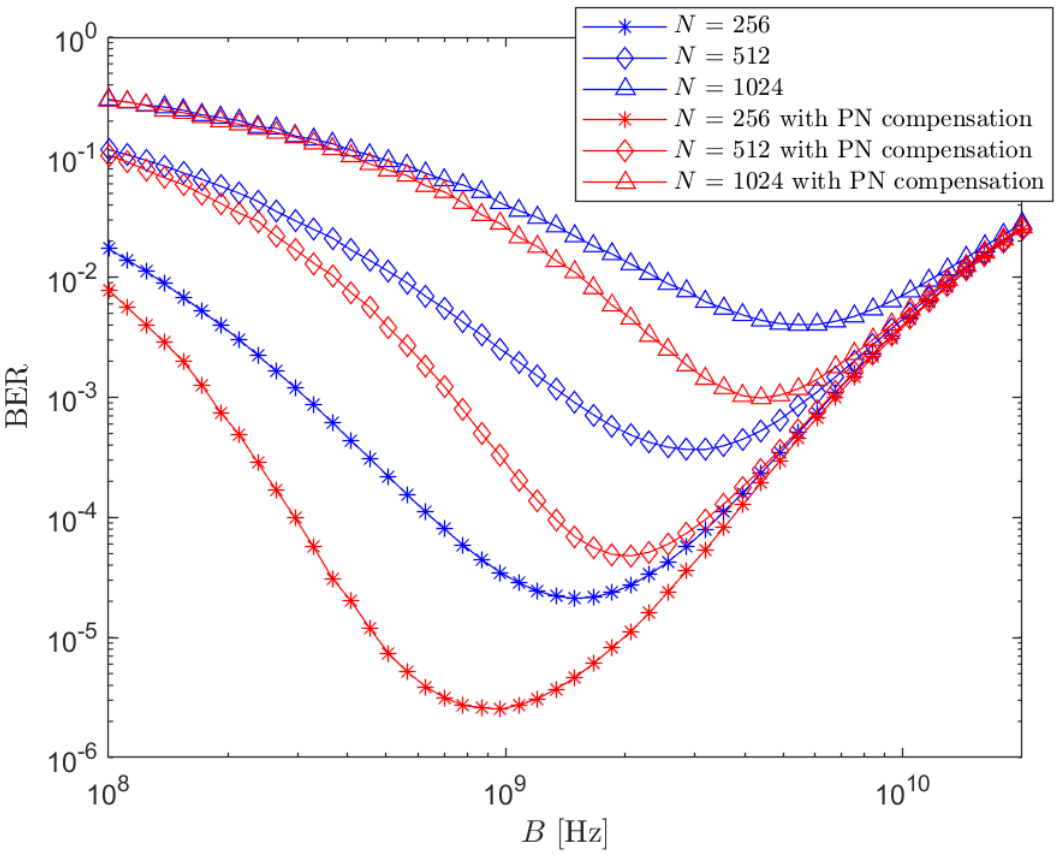

Figure 22: BER *vs B.* f_c*=1 MHz,* K_0*= -110 dBc,* SNR *= 15 dB and N = 256, 512, 1024.*

In Figure 22 the results are presented, together with the ones without compensation. As we can see, BER is reduced to about one tenth after the compensation, for the optimum value of *B*. The magnitude of improvement depends on *B*: the nearer it is to the optimum, the greater the improvement is. As we can see, with B = 10 GHz (the value considered in the previous simulation), the value on N that has the greatest improvement is N = 1024, a result coherent with the one of the tenth simulation (Figure 21).

We can understand the behaviour of the system as follow: let us consider a certain curve, e.g., the one for N = 256, and a target value of BER, e.g., 10^{-4}. Then, let us choose the lowest value of *B* for which the target BER is obtained in the absence of compensation. As we can see, after compensation, the corresponding value of *B* is lower. As it is suggested by (4.1), the lower is *B*, the smaller is the spacing between the chirps: this means that, thanks to the compensation, the system manage to obtain the same performance with a lower spacing between chirps.

Conclusions

In the first chapter, Beyond 5G and Terahertz communications have been introduced, highlighting which are the possibility that they can provide, and which are the main issues that afflict them.

In the second chapter, the phase noise has been studied, focusing on how it is generated and on how it can be modelled. Considerations and analysis were made to model the noise at Terahertz frequency as white and Gaussian: this allowed us to model the phase noise as the superposition of two components, the Wiener one and the white one.

In the third chapter, OCDM has been introduced, along with the analytical expression of the received signal affected by phase noise. This allowed to distinguish two phase noise components: the Common Phase Error (CPE) and the Inter-Chirp Interference (ICI). A simple compensation algorithm for CPE, originally introduced for OFDM systems, has been reported.

In the fourth chapter, numerical results have been shown. It has been found that the performance of the system, in terms of BER, depends on the number of chirps N. The dependence on other parameters was also found, the most significant being the frequency deviation B: there is an optimum value of B that, for a given SNR, minimizes BER. This phenomenon is due to the fact that with a small B, chirps are more compressed and phase noise easily cause error at the detection, while with a large B, a larger amount of noise (that is converted into phase noise) affects the system. The trade-off between those two is the reason why an optimum value can be found. This value also depends on N.
A simple compensation algorithm has been applied to the system: BER has improved, and the magnitude of the improvement depends on B as well. In particular, it is greater when B is near to the optimum value. It has been found that BER could be reduced to one tenth of the original value.

References

[1] M. Chiani, E. Paolini and F. Callegati, “Open issues and beyond 5G,” 2020. [Online]. Available: https://www.5gitaly.eu/2018/wp-content/uploads/2019/01/5G-Italy-White-eBook-Beyond-5G.pdf.

[2] X. Ouyang and J. Zhao, “Orthogonal Chirp Division Multiplexing”.

[3] Ericsson , “Ericsson Mobility Report,” June 2021. [Online]. Available: https://www.ericsson.com/en/mobility-report.

[4] GSMA, “The Mobile Economy 2021,” 2021. [Online]. Available: https://www.gsma.com/mobileeconomy/.

[5] ITU, “Minimum requirements related to technical performance for IMT-2020 radio interface(s),” 2017. [Online]. Available: https://www.itu.int/pub/R-REP-M.2410-2017.

[6] 5G-PPP, “White Paper - 5G and the Factories of the Future,” 2015. [Online]. Available: https://5g-ppp.eu/wp-content/uploads/2014/02/5G-PPP-White-Paper-on-Factories-of-the-Future-Vertical-Sector.pdf.

[7] 5G ACIA, “White Paper - 5G for Connected Industries and Automation,” 2019. [Online]. Available: https://5g-acia.org/wp-content/uploads/2021/04/WP_5G_for_Connected_Industries_and_Automation_Download_19.03.19.pdf.

[8] NGMN, “5G E2E technology to support verticals URLLC requirements,” 2019. [Online]. Available: https://www.ngmn.org/wp-content/uploads/200210-Verticals-URLLC-Requirements-v2.5.4.pdf.

[9] T. Le, U. Salim and F. Kaltenberger, “An Overview of Physical Layer Design for Ultra-Reliable Low-Latency Communicationsin 3GPP Releases 15, 16, and 17,” 2020.

[10] Ericsson, “Mobile data traffic outlook,” [Online]. Available: https://www.ericsson.com/en/mobility-report/dataforecasts/mobile-traffic-forecast.

[11] Opensignal, “The 5G opportunity – how 5G will solve the congestion problems of today’s 4G networks,” 2019. [Online]. Available: https://www.opensignal.com/reports/2019/02/global-state-of-the-mobile-network.

[12] H. Elayan, O. Amin, R. M. Shubair and M. Alouini, “Terahertz communication: The opportunities of wireless technology beyond 5G,” Marrakech, Morocco, 2018.

[13] J. M. Jornet and I. F. Akyildiz, “Channel Modeling and Capacity Analysis for Electromagnetic Wireless Nanonetworks in the Terahertz Band,” 2011.

[14] S. Ghafoor, N. Boujnah, M. H. Rehmani and A. Davy, “MAC Protocols for Terahertz Communication: A Comprehensive Survey,” 2019.

[15] C. Buratti, L. Mesini and R. Verdone, “Comparing MAC Protocols for Industrial IoT Using Terahertz Communications,” 2020.

[16] S. Dang, O. Amin, B. Shihada and M.-S. Alouini, “Whay Should 6G Be?,” 2020.

[17] S. Rommel, T. R. Raddo and I. T. Monroy, “Data Center Connectivity by 6G Wireless Systems,” 2018.

[18] V. P. A. Petrov, D. Moltchanov and Y. Koucheryavy, “Terahertz Band Communications: Applications, Research Challenges, and Standardization Activities,” 2020.

[19] A. Hajimiri and T. H. Lee, “A General Theory of Phase Noise in Electrical Oscillators,” 1998.

[20] Texas Instruments , *Fractional/Integer-N PLL Basics,* 1999.

[21] IEEE, *IEEE Standard Definitions of Physical Quantities for Fundamental Frequency and Time Metrology - Random Instabilities,* 2009.

[22] S. Bicais and J.-B. Dore, “Phase Noise Model Selection for Sub-THz Communications,” 2019.

[23] A. Demir, “Computing Timing Jitter From Phase Noise Spectra for Oscillators and Phase-Locked Loops With White and 1/f Noise,” 2006.

[24] B. Razavi, RF Microelectronics, 1997.

[25] M. R. Khanzadi, *Phase Noise in Communication Systems: Modeling, Compensation, and Performance Analysis,* 2015.

[26] L. Calandrino and M. Chiani, Lezioni di Comunicazioni Elettriche.

[27] R. Bomfin, M. Chafii and G. Fettweis, “Coding, Performance Assessment of Orthogonal Chirp Division Multiplexing in MIMO Space Time,” 2019.

[28] C. Browning, X. Ouyang, D. Dass, G. Talli and P. Townsend, “Orthogonal Chirp-Division Multiplexing for Performance Enhanced Optical/Millimeter-Wave 5G/6G Communications”.

[29] M. Noroozi, A. Zahedi and H. Bakhshi, “Compensation of phase noise in OFDM systems using a CPE and channel estimation scheme,” 2008.

[30] V. Abhayawardhana and I. Wassell, *Common Phase Error Correction for OFDM in Wireless Communication,* 2002.

[31] Y. Zhao, Z.-Z. Chen, Y. Du, Y. Li, R. Al Hadi, G. Virbila, Y. Xu, K. Yanghyo, A. Tang, T. Reck and M.-C. F. Chang, “A 0.56 THz Phase-Locked Frequency Synthesizer in 65 nm CMOS Technology,” 2016.

[32] L. Yi, K. Iwamoto, T. Yamamoto, F. Ayano, A. Rolland, N. Kuse, M. Fermann, Y. Li and T. Nagatsuma, “300-GHz-band wireless communication using a low phase noise photonic source”.

Figure index